Wave Motion 62 (2016) 75–97

Contents lists available at ScienceDirect

Wave Motion

journal homepage: www.elsevier.com/locate/wavemoti

Solving the Helmholtz equation for general smooth geometry using simple grids[☆]

M. Medvinsky[a,∗], S. Tsynkov[b,c], E. Turkel[d]

[a] Department of Mathematics, University of Utah, Salt Lake City, UT, USA
[b] Department of Mathematics, North Carolina State University, Box 8205, Raleigh, NC 27695, USA
[c] Moscow Institute of Physics and Technology, Dolgoprudny, 141700, Russia
[d] School of Mathematical Sciences, Tel Aviv University, Ramat Aviv, Tel Aviv 69978, Israel

HIGHLIGHTS

- Method of difference potentials applied to general geometry and multiple scattering.
- High order accurate numerical method for boundary value problems of wave motion.
- Includes transmission and scattering of acoustic and electromagnetic waves.
- Highly effective finite differences for complicated geometries and boundary condition.
- Curvilinear interfaces, variable coefficients using regular structured grid.

ARTICLE INFO

Article history:
Received 4 July 2015
Received in revised form 13 December 2015
Accepted 18 December 2015
Available online 30 December 2015

Keywords:
Difference potentials
Boundary projections
Calderon's operators
Curvilinear boundaries
High order compact differencing
Multiple scattering

ABSTRACT

The method of difference potentials was originally proposed by Ryaben'kii, and is a generalized discrete version of the method of Calderon's operators. It handles non-conforming curvilinear boundaries, variable coefficients, and non-standard boundary conditions while keeping the complexity of the solver at the level of a finite-difference scheme on a regular structured grid. Compact finite difference schemes enable high order accuracy on small stencils and so require no additional boundary conditions beyond those needed for the differential equation itself. Previously, we have used difference potentials combined with compact schemes for solving transmission/scattering problems in regions of a simple shape. In this paper, we generalize our previous work to incorporate smooth general shaped boundaries and interfaces, including a formulation that involves multiple scattering.

© 2015 Elsevier B.V. All rights reserved.

1. Introduction

We propose a high order accurate numerical method for the solution of two-dimensional boundary value problems of wave analysis. It applies to a wide variety of physical formulations that involve the transmission and scattering of acoustic and electromagnetic waves. In the current paper, we solve the scalar wave propagation problem in the frequency domain and concentrate on applications to general shaped boundaries and interfaces.

☆ Work supported by the US ARO, grant # W911NF-11-1-0384, and US–Israel BSF, grant # 2014048.

∗ Corresponding author.
E-mail addresses: medvinsky.michael@gmail.com (M. Medvinsky), tsynkov@math.ncsu.edu (S. Tsynkov), turkel@post.tau.ac.il (E. Turkel).
URL: http://www.math.ncsu.edu/~stsynkov (S. Tsynkov).

http://dx.doi.org/10.1016/j.wavemoti.2015.12.004
0165-2125/© 2015 Elsevier B.V. All rights reserved.

It is well known that high order accuracy is of central importance for the numerical simulation of waves because of the pollution effect [1–3]. For both finite difference and finite element approximations, the numerical phase velocity of the wave depends on the wavenumber k, so a propagating packet of waves with different frequencies gets distorted in the simulation. Furthermore, the numerical error is proportional to $h^p k^{p+1}$, where h is the grid size and p is the order of accuracy of the chosen approximation. So the number of points per wavelength needed for a given accuracy increases as $k^{1/p}$. Hence, higher order accurate approximations are very beneficial, as they reduce the effect of the pollution.

Our methodology for solving the Helmholtz equation combines compact equation-based high order accurate finite difference schemes [4,5] with the method of difference potentials by Ryaben'kii [6,7]. We have chosen this approach because we can take advantage of the simplicity and efficiency of high order finite difference schemes on regular structured grids (such as Cartesian or polar) and at the same time are able to handle non-conforming curvilinear boundaries and interfaces with no deterioration of accuracy due to staircasing.

The technique we propose presents a viable alternative to finite elements. Unlike finite differences, finite elements are designed for handling sophisticated geometries. However, high order accurate finite element approximations can be built for arbitrary boundaries only in fairly sophisticated and costly algorithms with isoparametric elements. These methods require grid generation which can be nontrivial for complex geometries and interfaces. In discontinuous Galerkin, discontinuous enrichment, and generalized finite element methods, high order accuracy also requires additional degrees of freedom. Yet, we are interested in predominantly smooth problems: geometrically large regions with smooth material parameters separated by several interface boundaries, e.g., scatterers in large volumes of free space. The solution of such problems is smooth between the interfaces (as long as the latter are sufficiently smooth in their own right) and so high order finite elements carry a substantial redundancy. The latter entails additional computational costs that we would like to avoid.

Therefore, we use compact finite difference schemes [8,9,4,5,10–12] to achieve high order accuracy. As any finite difference scheme, a compact scheme requires only one unknown per grid node, so there are no extra degrees of freedom. At the same time, unlike the standard high order accurate schemes compact schemes do not need extended stencils. In particular, equation-based compact schemes [4,5] use the equation itself to eliminate the distant stencil points. These high order schemes reduce pollution while keeping the treatment of the boundary conditions simple, since the order of the resulting difference equation is equal to the order of the differential equation. Hence, no additional numerical boundary conditions are required.

The previous stages of development of our computational approach are reported in a series of papers [13–18]. The method of difference potentials [6,7] furnishes the required geometric flexibility. Specifically, it applies to a discretization on a regular structured grid and allows for non-conforming curvilinear boundaries with no loss of accuracy. Our technique provides an attractive substitute for the method of boundary elements, because it is not limited to constant coefficients and does not involve singular integrals.

The method of difference potentials is a discrete analog of the method of Calderon's operators [19,20,7]. It has the following key advantages:

- Maximum generality of boundary conditions. Any type of boundary conditions can be handled with equal ease, including mixed, nonlocal and interfaces.
- The problem is discretized on a regular structured grid, yet boundaries and interfaces can have an arbitrary shape and need not conform to the grid. This causes no loss of accuracy due to staircasing.
- Variable coefficients, or equivalently, heterogeneous media, are easily handled. The constructs of Calderon's operators remain essentially unchanged.
- The methodology does not require numerical approximation of singular integrals. The inverse operators used for computing the discrete counterparts to Calderon's potentials and projections, involve no convolutions or singularities and allow fast numerical computation. The well-posedness of the discrete problem is guaranteed.

Our previous papers on the subject [13–18] discussed model obstacles that were either circles or ellipses. The objective of this study is to include scatterers with more general smooth shapes and to allow for multiple scattering. The numerical results that we present demonstrate that this objective has been successfully achieved. Our algorithm attains the design fourth order accuracy when solving the transmission/scattering problems for a variety of non-conforming shapes, including the case of heterogeneous media.

1.1. *Outline of the paper*

In Section 3, we provide a brief account of the compact high order accurate equation-based schemes [4,5,8,9] for solving the variable coefficient Helmholtz equation. In Section 4, we introduce Calderon operators and their discrete counterparts. We briefly discuss their key properties. In Section 5 we discuss the coordinates associated with the interface curve and the equation-based extension. In Section 6, we present the results of computations confirming the high order accuracy for non-conforming boundaries. Finally, Section 7 contains conclusions.

2. Formulation of the problem

The most general problem formulation that we study in the paper involves embedded regions and allows for multiple

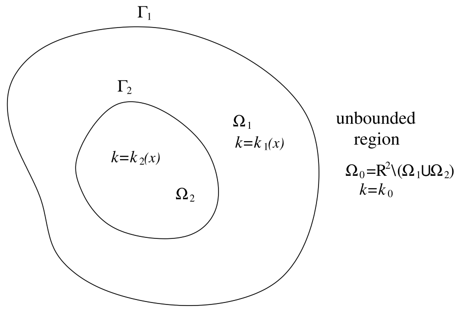

Fig. 1. Schematic for the transmission/reflection problem that involves multiple scattering.

scattering, see Fig. 1. Let Γ_1 and Γ_2 be two non-intersecting smooth closed curves inside one another. They partition the plane $\mathbb{R}^2$ into three regions: the exterior region Ω_0, which is outside Γ_1, the intermediate region Ω_1, which is in-between Γ_1 and Γ_2, and the interior region Ω_2, which is inside Γ_2. Then, $\partial\Omega_0 = \Gamma_1$, $\partial\Omega_1 = \Gamma_1 \cup \Gamma_2$, and $\partial\Omega_2 = \Gamma_2$.

We consider the time-harmonic waves propagating in an unbounded heterogeneous medium defined by the domains Ω_0, Ω_1, and Ω_2. The propagation is governed by the scalar Helmholtz equation. In the exterior domain Ω_0, the wavenumber k in the Helmholtz equation (which is determined by the local propagation speed, $k = \omega/c$) is assumed constant, whereas in the intermediate domain Ω_1, as well as in the interior domain Ω_2, the wavenumber is allowed to vary smoothly:

$$k = k(\boldsymbol{x}) = \begin{cases} k_0, & \boldsymbol{x} \in \Omega_0, \\ k_1(\boldsymbol{x}), & \boldsymbol{x} \in \Omega_1, \\ k_2(\boldsymbol{x}), & \boldsymbol{x} \in \Omega_2 = \mathbb{R}^2 \setminus (\Omega_1 \cup \Omega_2). \end{cases} \tag{1}$$

At the boundaries Γ_1 and Γ_2, the wavenumber may undergo jump discontinuities, so that altogether the function $k = k(\boldsymbol{x})$ of (1) is piecewise smooth.

The Helmholtz equation for the medium with $k(\boldsymbol{x})$ given by (1) is written in the form of three individual sub-equations that correspond to the regions where the wavenumber varies smoothly:

$$\boldsymbol{L}_2 u \stackrel{\text{def}}{=} \Delta u(\boldsymbol{x}) + k_2^2(\boldsymbol{x})u = f_2(\boldsymbol{x}), \quad \boldsymbol{x} \in \Omega_2, \tag{2a}$$

$$\boldsymbol{L}_1 u \stackrel{\text{def}}{=} \Delta u(\boldsymbol{x}) + k_1^2(\boldsymbol{x})u = f_1(\boldsymbol{x}), \quad \boldsymbol{x} \in \Omega_1, \tag{2b}$$

$$\boldsymbol{L}_0 u \stackrel{\text{def}}{=} \Delta u(\boldsymbol{x}) + k_0^2 u = f_0(\boldsymbol{x}), \quad \boldsymbol{x} \in \Omega_0. \tag{2c}$$

To ensure uniqueness, additional conditions must be specified at the interfaces Γ_1 and Γ_2 where the coefficient k undergoes jumps, as well as at infinity. We require that the function u and its first normal derivative be continuous across Γ_1 and Γ_2, and at infinity we impose the Sommerfeld radiation condition. The solution u of Eqs. (2) is assumed driven by the given incident plane wave $u^{(\text{inc})} = e^{-i\boldsymbol{k}\cdot\boldsymbol{x}}$, where $|\boldsymbol{k}| = k_0$, as well as by the source terms $f_q(\boldsymbol{x})$, $q \in \{0, 1, 2\}$.

For the numerical experiments of Section 6 that do not involve multiple scattering, the forgoing problem formulation is simplified. The interface Γ_2 and the separate interior domain Ω_2 are eliminated, so that $\Omega_0 = \mathbb{R}^2 \setminus \Omega_1$ and $\Gamma_1 = \partial\Omega_1 = \partial\Omega_0$. The domain Ω_1 becomes simply connected, and the wavenumber $k = k_1(\boldsymbol{x})$ varies smoothly across the entire Ω_1 Then, we are solving a typical transmission/reflection problem.

3. Compact high order accurate equation-based schemes

3.1. Scheme for the interior and intermediate problems

For the interior problem formulated on Ω_2 and the intermediate problem formulated on Ω_1, we consider the Helmholtz equation with a variable wavenumber (see Eqs. (2a), (2b)):

$$\boldsymbol{L}_q u \equiv \frac{\partial^2 u}{\partial x^2} + \frac{\partial^2 u}{\partial y^2} + k^2(x, y)u = f(x, y), \quad q \in \{1, 2\}, \tag{3}$$

where $k(x, y) = k_q(x, y)$, see (1), and $f(x, y) = f_q(x, y)$.

We introduce a uniform in each direction Cartesian grid with the sizes h_x and h_y and use the following equation-based compact scheme:

$$\frac{u_{i+1,j} - 2u_{i,j} + u_{i-1,j}}{h_x^2} + \frac{u_{i,j+1} - 2u_{i,j} + u_{i,j-1}}{h_y^2} + (k^2 u)_{i,j}$$

$$+\left(\frac{h_x^2}{12}+\frac{h_y^2}{12}\right)\frac{1}{h_x^2}\left(\frac{u_{i+1,j+1}-2u_{i+1,j}+u_{i+1,j-1}}{h_y^2}-2\frac{u_{i,j+1}-2u_{i,j}+u_{i,j-1}}{h_y^2}+\frac{u_{i-1,j+1}-2u_{i-1,j}+u_{i-1,j-1}}{h_y^2}\right)$$
$$+\frac{h_x^2}{12}\frac{(k^2u)_{i+1,j}-2(k^2u)_{i,j}+(k^2u)_{i-1,j}}{h_x^2}+\frac{h_y^2}{12}\frac{(k^2u)_{i,j+1}-2(k^2u)_{i,j}+(k^2u)_{i,j-1}}{h_y^2}$$
$$=\frac{h_x^2}{12}\frac{f_{i+1,j}-2f_{i,j}+f_{i-1,j}}{h_x^2}+\frac{h_y^2}{12}\frac{f_{i,j+1}-2f_{i,j}+f_{i,j-1}}{h_y^2}+f_{i,j}. \tag{4}$$

Details of the derivation and accuracy analysis can be found in [8,9,21,5]. The scheme yields fourth order accuracy for smooth solutions. Even higher accuracy can be achieved using the same compact stencils. In [21], we have constructed a sixth order accurate equation-based scheme for the Helmholtz equation with a variable wavenumber k. Unlike regular schemes, the compact scheme (4) employs two stencils. The nine-node 3×3 stencil $\{(i,j),(i\pm 1,j),(i,j\pm 1),(i\pm 1,j\pm 1)\}$ is used for the discrete solution $u_{i,j}$, and the five-node stencil $\{(i,j),(i\pm 1,j),(i,j\pm 1)\}$ is used for the source function $f_{i,j}$. Since the left-hand side stencil is 3×3, the compact scheme (4) does not require additional boundary conditions beyond those needed for the original differential equation. Dirichlet boundary conditions are straightforward to set; Neumann boundary conditions can also be included without expanding the stencil [9,21].

3.2. Scheme for the exterior problem

For the exterior problem formulated on Ω_0, we consider the Helmholtz equation with a constant wavenumber $k=k_0$ (see Eq. (2c)):

$$\boldsymbol{L}_0 u=\frac{1}{r}\frac{\partial}{\partial r}\left(r\frac{\partial u}{\partial r}\right)+\frac{1}{r^2}\frac{\partial^2 u}{\partial\theta^2}+k^2u=f(r,\theta). \tag{5}$$

The equation-based compact scheme is built on a uniform polar grid with the sizes h_r and h_θ:

$$\begin{aligned}
&\frac{1}{r_m}\frac{1}{h_r}\left(r_{m+1/2}\frac{u_{m+1,l}-u_{m,l}}{h_r}-r_{m-1/2}\frac{u_{m,l}-u_{m-1,l}}{h_r}\right)\\
&+\frac{1}{r_m^2}\frac{u_{m,l+1}-2u_{m,l}+u_{m,l-1}}{h_\theta^2}-\frac{h_r^2}{12}\left[\left.\frac{\partial^2 f}{\partial r^2}\right|_{m,l}-k^2\frac{u_{m+1,l}-2u_{m,l}+u_{m-1,l}}{h_r^2}\right]\\
&+\frac{1}{12h_\theta^2}\left[\frac{1}{r_{m+1}^2}\left(u_{m+1,l+1}-2u_{m+1,l}+u_{m+1,l-1}\right)\right.\\
&\left.-\frac{2}{r_m^2}\left(u_{m,l+1}-2u_{m,l}+u_{m,l-1}\right)+\frac{1}{r_{m-1}^2}\left(u_{m-1,l+1}-2u_{m-1,l}+u_{m-1,l-1}\right)\right]\\
&-\frac{h_r^2}{12r_m}\left[\left.\frac{\partial f}{\partial r}\right|_{m,l}-k^2\frac{u_{m+1,l}-u_{m-1,l}}{2h_r}-\frac{1}{2h_rh_\theta^2}\left(\frac{1}{r_{m+1}^2}\left(u_{m+1,l+1}-2u_{m+1,l}+u_{m+1,l-1}\right)\right.\right.\\
&\left.\left.-\frac{1}{r_{m-1}^2}\left(u_{m-1,l+1}-2u_{m-1,l}+u_{m-1,l-1}\right)\right)\right]\\
&-\frac{h_r^2}{12r_m^2}\left(f_{m,l}-k^2u_{m,l}-\frac{1}{r_m^2h_\theta^2}\left(u_{m,l+1}-2u_{m,l}+u_{m,l-1}\right)\right)+\frac{h_r}{12r_m^3}\left(u_{m+1,l}-u_{m-1,l}\right)\\
&-\frac{h_\theta^2}{12}\left[\left.\frac{\partial^2 f}{\partial\theta^2}\right|_{m,l}-k^2\frac{u_{m,l+1}-2u_{m,l}+u_{m,l-1}}{h_\theta^2}\right]\\
&+\frac{1}{12h_r^2r_m}\left[r_{m+1/2}(u_{m+1,l+1}-u_{m,l+1})-r_{m-1/2}(u_{m,l+1}-u_{m-1,l+1})\right.\\
&-2\left(r_{m+1/2}(u_{m+1,l}-u_{m,l})-r_{m-1/2}(u_{m,l}-u_{m-1,l})\right)\\
&\left.+r_{m+1/2}(u_{m+1,l-1}-u_{m,l-1})-r_{m-1/2}(u_{m,l-1}-u_{m-1,l-1})\right]+k^2u_{m,l}=f_{m,l}.
\end{aligned} \tag{6}$$

Scheme (6) yields fourth order accuracy for smooth solutions; it is analyzed and tested in [4]. Similarly to scheme (4), the compact scheme (6) also employs two stencils. The stencil for the discrete solution $u_{m,l}$ is nine-node: $\{(m,l),(m\pm 1,l),(m,l\pm 1),(m\pm 1,l\pm 1)\}$, and the stencil for the right-hand side $f_{m,l}$ is five-node: $\{(m,l),(m\pm 1,l),(m,l\pm 1)\}$.

Scheme (6) requires no additional boundary conditions beyond those needed for the original differential equation, since the left-hand side stencil is 3×3. Neumann boundary conditions for scheme (6) can be set using the same 3×3 stencil, see [13].

4. Difference potentials and projections

4.1. Auxiliary problem

The original domains Ω_2, Ω_1 and Ω_0, see (2), may have a general irregular shape. This could make setting the boundary conditions for schemes (4) and (6), respectively, difficult, given that both schemes are constructed on regular structured grids. The method of difference potentials, however, allows us to completely circumvent those difficulties.

We enclose each domain $\Omega_j, j \in \{0, 1, 2\}$, within an auxiliary domain $\widetilde{\Omega}_j$: $\Omega_j \subset \widetilde{\Omega}_j$. On the domain $\widetilde{\Omega}_j$, we formulate a special auxiliary problem (AP) for the corresponding inhomogeneous Helmholtz equation. The key requirement of the AP is that it should have a unique solution for any right-hand side defined on $\widetilde{\Omega}_j$. It can otherwise be formulated arbitrarily except that the exterior AP needs to include an exact or approximate counterpart of the Sommerfeld radiation condition. Hence, we choose the AP so that it is easy to solve numerically. In particular, we select the auxiliary domains of simple shape, rectangular for $\widetilde{\Omega}_2$ and $\widetilde{\Omega}_1$, and annular for $\widetilde{\Omega}_0$. In the method of difference potentials, the AP is used for computing the discrete counterparts of Calderon's operators [19,20]. While the operators themselves depend on the choice of the AP, the actual solution u of the problem of interest, e.g., the interface problem (2), is not affected [7].

4.1.1. Interior and intermediate AP

The interior and intermediate auxiliary problems are formulated using Cartesian coordinates on the rectangular domain $\widetilde{\Omega}_q = [x_0^q, x_1^q] \times [y_0^q, y_1^q]$, $q \in \{1, 2\}$:

$$\begin{aligned} &\boldsymbol{L}_q u = g^q, && x \in \widetilde{\Omega}_q,\\ &u = 0, && y \in \{y_0^q, y_1^q\},\\ &\frac{\partial u}{\partial x} = i\mu u, && x = x_0^q,\\ &-\frac{\partial u}{\partial x} = i\mu u, && x = x_1^q. \end{aligned} \tag{7}$$

In doing so, we are assuming that the variable coefficient k_q is defined not only on Ω_q, but on the larger domain $\widetilde{\Omega}_q$ as well. The AP (7) is approximated by means of the compact scheme (4) and then solved by LU decomposition. In Section 4.2, we will see that the algorithm requires repeated solution of the AP for one and the same operator and different right-hand sides. This allows us to perform the LU decomposition only once and thus achieve substantial gains in performance. In the particular case where $k_q = \text{const}$, the AP (7) can be solved using the separation of variables and FFT. Note that the complex Robin boundary conditions imposed at the left and right boundaries of the auxiliary domain $\widetilde{\Omega}_q$, $q \in \{1, 2\}$, are not intended to represent any physical behavior. They merely make the spectrum of the AP complex and hence ensure the uniqueness of the solution. These boundary conditions can be approximated with fourth order accuracy without having to extend the compact stencil of the scheme (4), see [5, Section 4.2].

Let $\mathbb{N}_q$, $q \in \{1, 2\}$ be a uniform Cartesian grid on the rectangle $\widetilde{\Omega}_q$:

$$\mathbb{N}_q = \left\{(x_m^q, y_n^q) \mid x_m^q = mh^q,\ y_n^q = nh^q,\ m = 0, \dots, M_q,\ n = 0, \dots, N_q\right\}.$$

Creating a discrete analog of the boundary $\partial\Omega_q$ is central to our method since $\partial\Omega_q$ is not aligned with the Cartesian grid.[1] The following subsets of the Cartesian grid $\mathbb{N}_q$ are used for this purpose. Let $\mathbb{M}_q \subset \mathbb{N}_q$ be the set of only interior nodes of the rectangular domain $\widetilde{\Omega}_q$. Thus $\mathbb{M}_q$ contains all the nodes of $\mathbb{N}_q$ except for those along the boundary edges of the rectangle:

$$\mathbb{M}_q = \left\{(x_m^q, y_n^q) \mid x_m^q = mh^q,\ y_n^q = nh^q,\ m = 1, \dots, M_q - 1,\ n = 1, \dots, N_q - 1\right\}.$$

Notice, that if we form a set which contains all of the nodes "touched" by the 9-point compact stencil operating on the set $\mathbb{M}_q$, then this set will coincide with $\mathbb{N}_q$. It is for this reason that the right-hand side $g_{m,n}^q$ of the discrete AP is defined only on the interior nodes, i.e., on $\mathbb{M}_q$. We now distinguish those nodes which are within the domain Ω_q from those which are not in Ω_q. For $q = 1$, being in Ω_1 means in-between the curves Γ_1 and Γ_2; for $q = 2$, being in Ω_2 means inside the curve Γ_2. Let all those nodes which belong to Ω_q be denoted by $\mathbb{M}_q^+ \subset \mathbb{M}_q$, and those which do not belong to Ω_q, except for the edges of the auxiliary domain, by $\mathbb{M}_q^- \subset \mathbb{M}_q$. Next, let the collections of all nodes touched by the 9-point compact stencil operating on the nodes of $\mathbb{M}_q^+$ and $\mathbb{M}_q^-$ be referred to as $\mathbb{N}_q^+$ and $\mathbb{N}_q^-$, respectively. Then, there is a nonempty intersection between the sets $\mathbb{N}_q^+$ and $\mathbb{N}_q^-$. This is referred to as the grid boundary:

$$\gamma_q = \mathbb{N}_q^+ \cap \mathbb{N}_q^-, \quad q \in \{1, 2\}. \tag{8}$$

[1] Recall, $\partial\Omega_2 = \Gamma_2$ and $\partial\Omega_1 = \Gamma_2 \cup \Gamma_1$, see Fig. 1.

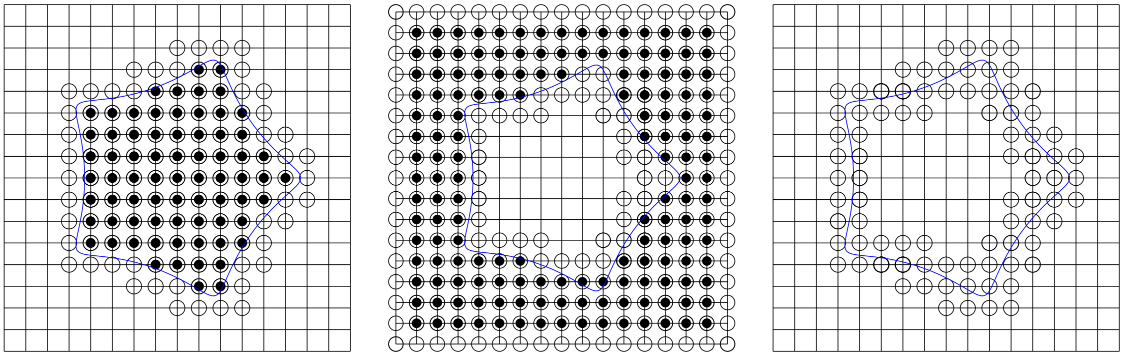

(a) • − $\mathbb{M}_2^+$, ○ − $\mathbb{N}_2^+$. (b) • − $\mathbb{M}_2^-$, ○ − $\mathbb{N}_2^-$. (c) ○ − γ_2.

Fig. 2. Interior and exterior grid subsets and the grid boundary for the interior sub-problem.

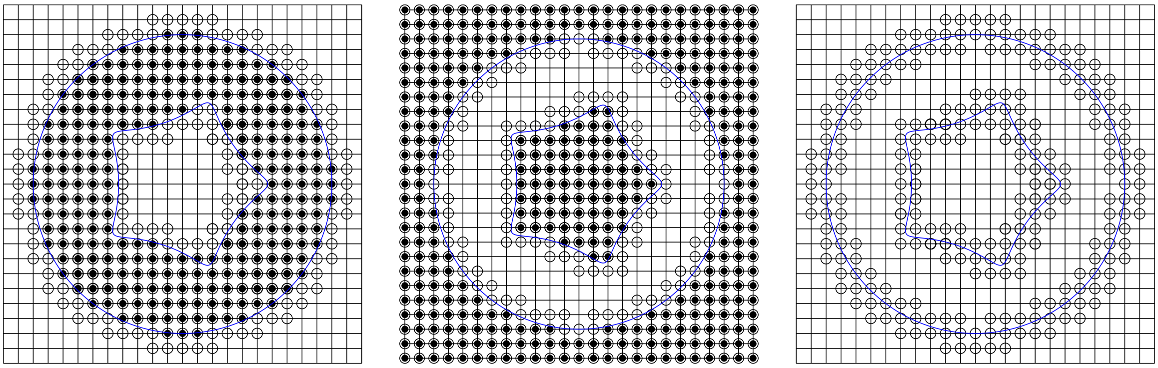

(a) • − $\mathbb{M}_1^+$, ○ − $\mathbb{N}_1^+$. (b) • − $\mathbb{M}_1^-$, ○ − $\mathbb{N}_1^-$. (c) ○ − γ_1.

Fig. 3. Interior and exterior grid subsets and the grid boundary for the intermediate sub-problem.

Examples for all the foregoing grid sets are shown in Figs. 2 and 3. Let us emphasize that the grid sets for different values of q ($q = 1$ and $q = 2$) are constructed completely independently; already at the very first step the grids $\mathbb{N}_1$ and $\mathbb{N}_2$ can be different. As such, the interior part of γ_1, see Fig. 3(c), may but does not have to coincide with γ_2 shown in Fig. 2(c).

4.1.2. Exterior AP

The domain of the exterior problem is $\Omega_0 = \mathbb{R}^2 \setminus (\Omega_1 \cup \Omega_2)$. The corresponding auxiliary domain $\widetilde{\Omega}_0$ is chosen to be the annulus $\{r_0 \leqslant r \equiv |\boldsymbol{x}| \leqslant r_1\}$ that contains the interface curve Γ_1. Then, we formulate the exterior AP as follows:

$$\begin{aligned} \boldsymbol{L}_0 u &= g_0, & r_0 < r &= |\boldsymbol{x}| < r_1, \\ u &= 0, & r &= r_0, \\ \boldsymbol{T} u &= 0, & r &= r_1. \end{aligned} \tag{9}$$

The operator boundary condition $\boldsymbol{T}u = 0$ in (9) is equivalent to the Sommerfeld radiation condition, but set at the finite boundary $r = r_1$ rather than at infinity. The operator $\boldsymbol{T}$ can be explicitly constructed in the transformed space after the variables in problem (9) have been separated by means of the azimuthal Fourier transform. In doing so, the entire AP (9) is also solved by separation of variables, which leads to a very efficient numerical procedure, see [4, Section 4].

We denote by $\mathbb{N}_0$ the uniform polar grid on the annulus $\widetilde{\Omega}_0$:

$$\mathbb{N}_0 = \left\{(r_m, \theta_n) \mid r_m = mh,\ \theta_n = nh,\ m = 0, \dots, M_0,\ n = 0, \dots, N_0\right\}.$$

A discrete analog of the boundary curve $\Gamma_1 = \partial\Omega_0$ for the polar grid is defined similarly to that for the Cartesian grid. Namely, let $\mathbb{M}_0 \subset \mathbb{N}_0$ be the set of only interior nodes of the polar domain $\widetilde{\Omega}_0$:

$$\mathbb{M}_0 = \left\{(r_m, \theta_n) \mid r_m = mh,\ \theta_n = nh,\ m = 1, \dots, M_0 - 1,\ n = 1, \dots, N_0 - 1\right\}.$$

Let all of those nodes which are confined within the continuous boundary Γ_1 be denoted by $\mathbb{M}_0^+ \subset \mathbb{M}_0$, and those which are outside, except for the edges of the auxiliary domain, by $\mathbb{M}_0^- \subset \mathbb{M}_0$. Next, let the collections of all nodes touched by the 9-point compact stencil operating on the nodes of $\mathbb{M}_0^+$ and $\mathbb{M}_0^-$ be referred to as $\mathbb{N}_0^+$ and $\mathbb{N}_0^-$, respectively. The intersection of the sets $\mathbb{N}_0^+$ and $\mathbb{N}_0^-$ is nonempty. The grid boundary is given by

$$\gamma_0 = \mathbb{N}_0^+ \cap \mathbb{N}_0^-. \tag{10}$$

The polar grid sets are shown in Fig. 4.

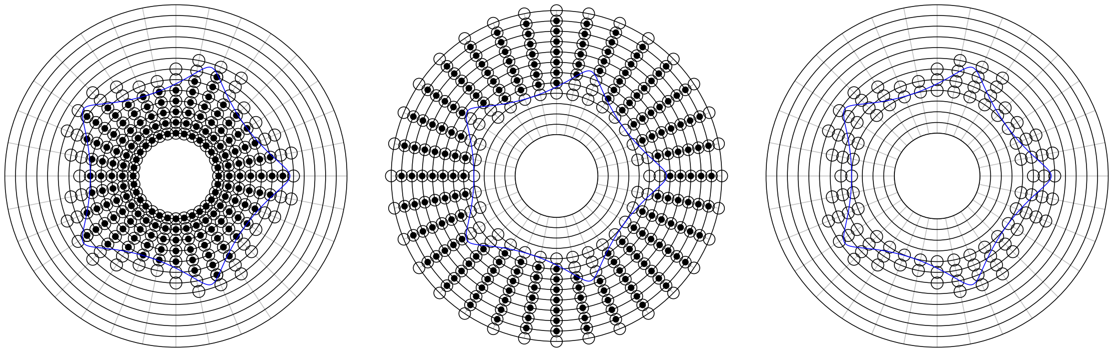

(a) $\bullet - \mathbb{M}_0^+$, $\bigcirc - \mathbb{N}_0^+$. (b) $\bullet - \mathbb{M}_0^-$, $\bigcirc - \mathbb{N}_0^-$. (c) $\bigcirc - \gamma_0$.

Fig. 4. Interior and exterior grid subsets and the grid boundary for the exterior sub-problem.

4.1.3. The grid boundary γ for general shapes

The key factor in obtaining γ_q by means of formulae (8) or (10) is the decision whether a given grid node is interior or exterior to the body enclosed by a given closed curve Γ, which can be either Γ_1 or Γ_2. This helps us define the sets $\mathbb{M}_q^+$, $\mathbb{M}_q^-$, $q \in \{0, 1, 2\}$, which, in turn, are used to obtain the sets $\mathbb{N}_q^+$ and $\mathbb{N}_q^-$, and hence, the set γ_q.

Regardless of the choice of grid such a decision is simple for a circle with a given radius R_0 centered at the origin, e.g., $\mathbb{M}_q^+ = \{(x, y)|\sqrt{x^2+y^2} \leqslant R_0\}$. It is similarly simple for ellipses of a given eccentricity e_0 centered at the origin, e.g., $\mathbb{M}_q^+ = \{(x, y)|\mathrm{Re}\,\mathrm{acosh}(x+iy) \leqslant \mathrm{acosh}\, e_0^{-1}\}$.

We now describe the procedure for a general shaped boundary Γ. Let $\boldsymbol{R} = (R_x(t), R_y(t))$ be the parameterization of a star-shaped interface/boundary Γ. Let $p = (x, y)$ be a grid point. In order to decide whether p is exterior or interior with respect to Γ, one compares the magnitude of the vector from the origin to the point p and the value of $\boldsymbol{R}$ in the same direction/angle θ. The curve $\boldsymbol{R}$ is a known function of the parameter t where in general $t \neq \theta$. To match between t and θ one uses a root finding algorithm, e.g., Newton–Raphson, to solve

$$\cos\frac{y}{x} = \cos\frac{R_y(t)}{R_x(t)} \tag{11}$$

for t. Once the matching is found the point $p = (x, y)$ is interior if it satisfies

$$\sqrt{x^2+y^2} < \sqrt{R_x^2(t(\theta)) + R_y^2(t(\theta))},$$

otherwise p is exterior.

4.2. Difference potentials

We now provide a brief description of the difference potentials and projections, while referring the reader to [7,13,14,22] for a comprehensive account of the methodology. In particular, the well-posedness is discussed in [13, Section 3.1.4] and in [7, Part I]. The accuracy was investigated by Reznik [23], and some results are outlined in [13, Section 4.4]. The complexity is analyzed in [13, Section 4.6]. Solutions of some exterior and interface problems are presented in [14]. Algorithms and examples can be found in [22].

Let ξ_{γ_q}, $q \in \{1, 2\}$, be a function specified at the grid boundary γ_q of (8). Let w^q be a grid function on $\mathbb{N}_q$ that satisfies the discretized boundary conditions of the interior AP (7) at $\partial\widetilde{\Omega}_q$, and also $w^q|_{\gamma_q} = \xi_{\gamma_q} \Leftrightarrow \boldsymbol{Tr}_{\gamma_q}^{(h)} w^q = \xi_{\gamma_q}$. The difference potential with density ξ_{γ_q} is defined as

$$\boldsymbol{P}_{\mathbb{N}_q^+}\xi_{\gamma_q} = w^q - \boldsymbol{G}_q^{(h)}\left(\boldsymbol{L}_q^{(h)} w^q\big|_{\mathbb{M}_q^+}\right), \quad n \in \mathbb{N}_q^+, \tag{12}$$

where $\boldsymbol{L}_q^{(h)}$ is the discrete counterpart of the continuous operator $\boldsymbol{L}_q$ of (7) or (3) and $\boldsymbol{G}_q^{(h)}$ is its inverse obtained by solving the interior difference AP of Section 4.1.1 on the grid $\mathbb{N}_q$. Accordingly, the difference boundary projection is given by $\boldsymbol{P}_{\gamma_q}\xi_{\gamma_q} = \boldsymbol{Tr}_{\gamma_q}^{(h)}\boldsymbol{P}_{\mathbb{N}_q^+}\xi_{\gamma_q}$. The key property of the projection $\boldsymbol{P}_{\gamma_q}$ is that a given ξ_{γ_q} satisfies the difference boundary equation with projection (BEP):

$$\boldsymbol{P}_{\gamma_q}\xi_{\gamma_q} + \boldsymbol{Tr}_{\gamma_q}^{(h)}\boldsymbol{G}_q^{(h)} f_q^{(h)} = \xi_{\gamma_q} \tag{13}$$

iff there exists u on $\mathbb{N}_q^+$ that satisfies Eq. (4) on $\mathbb{M}_q^+$ and such that $\boldsymbol{Tr}^{(h)}u = \xi_{\gamma_q}$. Note, that $f_q^{(h)}$ in formula (13) is the discrete source term of the Helmholtz equation after the application of the second, i.e., five-node, stencil of the compact scheme, see the right-hand side of Eq. (4).

The constructs of discrete operators for the exterior domain exploit the grid sets and the auxiliary problem introduced in Section 4.1.2. The potential on $\mathbb{N}_0^-$ is given by

$$\boldsymbol{P}_{\mathbb{N}_0^-}\xi_{\gamma_0} = w - \boldsymbol{G}_0^{(h)}\left(\boldsymbol{L}_0^{(h)} w\big|_{\mathbb{M}_0^-}\right), \tag{14}$$

and the projection on γ_0 is defined as $\boldsymbol{P}_{\gamma_0}\xi_{\gamma_0} = \boldsymbol{Tr}_{\gamma_0}^{(h)}\boldsymbol{P}_{\mathbb{N}_0^-}\xi_{\gamma_0}$, so that the discrete exterior BEP becomes

$$\boldsymbol{P}_{\gamma_0}\xi_{\gamma_0} + \boldsymbol{Tr}_{\gamma_0}^{(h)}\boldsymbol{G}_0^{(h)}f_0^{(h)} + (\boldsymbol{I} - \boldsymbol{P}_{\gamma_0})\boldsymbol{Tr}_{\gamma_0}^{(h)}u^{(\mathrm{inc})} = \xi_{\gamma_0}. \tag{15}$$

The method of difference potentials requires no approximation of the boundary or interface conditions on the grid, and avoids unwanted staircasing effects [24,25]. Let $\boldsymbol{\xi}_\Gamma = (\xi_0, \xi_1, \xi_2, \xi_3)|_\Gamma$ be the unknown vector function defined at the continuous boundary Γ. Unlike in Section 4.1.3 where Γ could be either Γ_1 or Γ_2, in this section $\Gamma = \Gamma_1 \cup \Gamma_2$, i.e. the union of both interfaces. We think of $\boldsymbol{\xi}_\Gamma$ as of the trace of the solution u and its first normal derivative. Suppose $\boldsymbol{\xi}_\Gamma$ has an expansion with respect to some basis $\{\psi_n\}$ (Fourier or Chebyshev) chosen on Γ:

$$\begin{aligned}\boldsymbol{\xi}_\Gamma = (\xi_0, \xi_1, \xi_2, \xi_3)\big|_\Gamma &= \underbrace{\sum_{n=-M}^{M} c_n^{(0)}(\psi_n, 0, 0, 0)}_{(\xi_0,0)} + \underbrace{\sum_{n=-M}^{M} c_n^{(1)}(0, \psi_n, 0, 0)}_{(0,\xi_1)} \\ &\quad + \underbrace{\sum_{n=-M}^{M} c_n^{(2)}(0, 0, \psi_n, 0)}_{(\xi_2,0)} + \underbrace{\sum_{n=-M}^{M} c_n^{(3)}(0, 0, 0, \psi_n)}_{(0,\xi_3)},\end{aligned} \tag{16}$$

where $c_n^{(0)}$, $c_n^{(1)}$, $c_n^{(2)}$ and $c_n^{(3)}$ are the coefficients to be determined. The summation in (16) can be taken finite because for sufficiently smooth $\boldsymbol{\xi}_\Gamma$ the corresponding Fourier or Chebyshev series converges rapidly. Hence, even for relatively small M the spectral representation (16) provides the accuracy beyond the one that can be obtained on the grid inside the computational domain.

Using Taylor's formula with equation-based derivatives [23,13,16], we extend $\boldsymbol{\xi}_\Gamma$ from Γ to the nodes of γ_q, $q \in \{1, 2\}$, located nearby:

$$\xi_{\gamma_2} = \boldsymbol{Ex}^{(2)}\boldsymbol{\xi}_\Gamma = \boldsymbol{Ex}_H^{(2)}(\xi_2, \xi_3)\big|_\Gamma + \boldsymbol{Ex}_I^{(2)}f_2, \tag{17}$$

$$\xi_{\gamma_1} = \boldsymbol{Ex}^{(1)}\boldsymbol{\xi}_\Gamma = \boldsymbol{Ex}_H^{(1)}(\xi_0, \xi_1, \xi_2, \xi_3)\big|_\Gamma + \boldsymbol{Ex}_I^{(1)}f_1. \tag{18}$$

Similarly for the exterior part, we introduce another equation-based Taylor extension:

$$\xi_{\gamma_0} = \boldsymbol{Ex}^{(0)}\boldsymbol{\xi}_\Gamma = \boldsymbol{Ex}_H^{(0)}(\xi_0, \xi_1)\big|_\Gamma + \boldsymbol{Ex}_I^{(0)}f_0. \tag{19}$$

In formulae (17), (18), and (19), the operators $\boldsymbol{Ex}_H^{(q)}$ and $\boldsymbol{Ex}_I^{(q)}$, $q \in \{0, 1, 2\}$, denote the homogeneous and inhomogeneous part of the overall extension, respectively. Taking $\boldsymbol{\xi}_\Gamma$ in the form (16), we rewrite (17)–(19) as follows:

$$\xi_{\gamma_2} = \boldsymbol{Ex}^{(2)}\boldsymbol{\xi}_\Gamma = \sum_{n=-M}^{M} c_n^{(2)}\boldsymbol{Ex}_H^{(2)}(0, 0, \psi_n, 0) + \sum_{n=M}^{M} c_n^{(3)}\boldsymbol{Ex}_H^{(2)}(0, 0, 0, \psi_n) + \boldsymbol{Ex}_I^{(2)}f_2,$$

$$\begin{aligned}\xi_{\gamma_1} = \boldsymbol{Ex}^{(1)}\boldsymbol{\xi}_\Gamma &= \sum_{n=-M}^{M} c_n^{(0)}\boldsymbol{Ex}_H^{(1)}(\psi_n, 0, 0, 0) + \sum_{n=M}^{M} c_n^{(1)}\boldsymbol{Ex}_H^{(1)}(0, \psi_n, 0, 0) \\ &\quad + \sum_{n=M}^{M} c_n^{(2)}\boldsymbol{Ex}_H^{(1)}(0, 0, \psi_n, 0) + \sum_{n=M}^{M} c_n^{(3)}\boldsymbol{Ex}_H^{(1)}(0, 0, 0, \psi_n) + \boldsymbol{Ex}_I^{(1)}f_1,\end{aligned}$$

and

$$\xi_{\gamma_0} = \boldsymbol{Ex}^{(0)}\boldsymbol{\xi}_\Gamma = \sum_{n=M}^{M} c_n^{(0)}\boldsymbol{Ex}_H^{(0)}(\psi_n, 0, 0, 0) + \sum_{n=M}^{M} c_n^{(1)}\boldsymbol{Ex}_H^{(0)}(0, \psi_n, 0, 0) + \boldsymbol{Ex}_I^{(0)}f_0.$$

Then, we substitute extensions (17), (18) into the BEP (13) and extension (19) into the BEP (15), which yields a system of linear equations to be solved with respect to the coefficients of (16):

$$\begin{bmatrix} \boldsymbol{Q}^{(0,2)} & \boldsymbol{Q}^{(1,2)} & 0 & 0 \\ \boldsymbol{Q}^{(0,1)} & \boldsymbol{Q}^{(1,1)} & \boldsymbol{Q}^{(2,1)} & \boldsymbol{Q}^{(3,1)} \\ 0 & 0 & \boldsymbol{Q}^{(2,0)} & \boldsymbol{Q}^{(3,0)} \end{bmatrix} \boldsymbol{c} = \begin{bmatrix} -\boldsymbol{Tr}_{\gamma_2}^{(h)}\boldsymbol{G}_2^{(h)}f_2^{(h)} - \left(\boldsymbol{P}_{\gamma_2} - \boldsymbol{I}\right)\boldsymbol{Ex}_I^{(2)}f_2 \\ -\boldsymbol{Tr}_{\gamma_1}^{(h)}\boldsymbol{G}_1^{(h)}f_1^{(h)} - \left(\boldsymbol{P}_{\gamma_1} - \boldsymbol{I}\right)\boldsymbol{Ex}_I^{(1)}f_1 \\ -\boldsymbol{Tr}_{\gamma_0}^{(h)}\boldsymbol{G}_0^{(h)}f_0^{(h)} - \left(\boldsymbol{P}_{\gamma_0} - \boldsymbol{I}\right)\left(\boldsymbol{Ex}_I^{(0)}f_0 - \boldsymbol{Tr}_{\gamma_0}^{(h)}u^{(\mathrm{inc})}\right) \end{bmatrix}. \tag{20}$$

In formula (20),

$$\boldsymbol{c} = \left[\boldsymbol{c}^{(0)}, \boldsymbol{c}^{(1)}, \boldsymbol{c}^{(2)}, \boldsymbol{c}^{(3)}\right]^T = \left[c_{-M}^{(0)}, \dots, c_{M}^{(0)}, c_{-M}^{(1)}, \dots, c_{M}^{(1)}, c_{-M}^{(2)}, \dots, c_{M}^{(2)}, c_{-M}^{(3)}, \dots, c_{M}^{(3)}\right]^T \tag{21}$$

and the columns of sub-matrices $\boldsymbol{Q}^{(p,q)}$, $p \in \{0, 1, 2, 3\}$, $q \in \{0, 1, 2\}$, are given by

$$\boldsymbol{Q}_n^{(p,q)} = \left(\boldsymbol{P}_{\gamma_q} - \boldsymbol{I}\right) \boldsymbol{Ex}_H^{(q)} \boldsymbol{\psi}_n^p,$$

where $\boldsymbol{\psi}_n^0 = (\psi_n, 0, 0, 0)$, $\boldsymbol{\psi}_n^1 = (0, \psi_n, 0, 0)$, $\boldsymbol{\psi}_n^2 = (0, 0, \psi_n, 0)$ and $\boldsymbol{\psi}_n^3 = (0, 0, 0, \psi_n)$, and $n = -M, \dots, M$. The number of rows in each matrix $\boldsymbol{Q}^{(p,q)}$ is equal to the number of nodes $|\gamma_q|$ in the grid boundary γ_q, $q \in \{0, 1, 2\}$. Hence, the overall vertical dimension of the matrix on the left-hand side of (20) is equal to $|\gamma_0| + |\gamma_1| + |\gamma_2|$.

We emphasize that since the same $\boldsymbol{\xi}_\Gamma$ appears in all Eqs. (17), (18), and (19), then the interface condition that requires the continuity of the solution u and its normal derivative across Γ (see the beginning of Section 3) is automatically enforced.

System (20) is typically overdetermined. It is solved with respect to $\boldsymbol{c}$ of (21) in the sense of least squares using QR decomposition. We note that even though the number of equations in system (20) exceeds the number of unknowns, its least squares solution is "almost classical" in the sense that the residual of (20) at the minimum is small and converges to zero as the grid size decreases. Finally, once $\boldsymbol{\xi}_\Gamma$ has been obtained in the form (16), we apply the extension operators (17), (18), and (19) once again and then compute the discrete interior and exterior solutions as the difference potentials (12) and (14), respectively.

The algorithm described in this section is simplified in the case of plain transmission/reflection problems that involve no multiple scattering. In this case, we have only two complementary domains, Ω_1 and $\Omega_0 = \mathbb{R}^2 \setminus \Omega_1$, and one interface Γ_1 separating them. The corresponding simplification is straightforward.

5. Coordinates associated with a curve and equation-based extension

The extension operators (17), (18), and (19) are of key significance for the application of the method of difference potentials. In this section, we construct these equation-based extensions on an arbitrarily shaped, yet smooth, simple closed interface curve Γ. This curve can be thought of as either Γ_1 or Γ_2 (similarly to Section 4.1.3). It is most natural to describe the extension in terms of the arc length parameterization of Γ. On the other hand, for a generally shaped curve it is often impossible to analytically obtain its arc length parameterization. Therefore, in many cases, it might be convenient to employ a different parameterization than arc length. Then, one would use the chain rule to obtain the required normal derivatives.

5.1. Curvilinear coordinates

Assume that Γ is parameterized by its arc length s:

$$\Gamma = \{\boldsymbol{R}(s) = (R_x(s), R_y(s)) | 0 \leqslant s \leqslant S\},$$

where $\boldsymbol{R}$ is the radius-vector that traces the curve. Assume, for definiteness, that as s increases the point $\boldsymbol{R}(s)$ moves counterclockwise along Γ. The unit tangent ($\boldsymbol{\tau}$) and the unit normal ($\boldsymbol{\nu}$) vectors to Γ are defined as

$$\boldsymbol{\tau} = \boldsymbol{\tau}(s) = \frac{d\boldsymbol{R}}{ds} \quad \text{and} \quad \boldsymbol{\nu} = (\nu_x, \nu_y) = (\tau_y, -\tau_x). \tag{22}$$

Given a counterclockwise parameterization $\boldsymbol{R} = \boldsymbol{R}(s)$, the normal $\boldsymbol{\nu}$ always points outward with respect to the domain Ω_1. Hence, the pair of vectors $(\boldsymbol{\nu}, \boldsymbol{\tau})$ always has a fixed right-handed orientation in the plane.

The relation between the tangent $\boldsymbol{\tau}$, the normal $\boldsymbol{\nu}$, and the curvature ζ of the curve Γ is given by the Frenet formula:

$$\frac{d\boldsymbol{\tau}}{ds} = \zeta \boldsymbol{\nu}. \tag{23}$$

The vector $\frac{d\boldsymbol{\tau}}{ds}$ is directed toward the center of curvature, i.e., it may point either toward Ω_1 or away from Ω_1 (i.e, toward Ω_0) depending on which direction the curve Γ bends. Since $\boldsymbol{\nu}$ has a fixed orientation, the curvature $\zeta = \zeta(s)$ in formula (23) should be taken with the sign (see, e.g., [26, Part 1]):

$$\zeta(s) = \begin{cases} \left|\dfrac{d\boldsymbol{\tau}}{ds}\right|, & \text{if } \dfrac{d\boldsymbol{\tau}}{ds} \cdot \boldsymbol{\nu} > 0, \\ -\left|\dfrac{d\boldsymbol{\tau}}{ds}\right|, & \text{if } \dfrac{d\boldsymbol{\tau}}{ds} \cdot \boldsymbol{\nu} < 0. \end{cases} \tag{24}$$

To define the coordinates associated with the curve Γ we take into account that the shortest path from a given node that belongs to the grid boundary γ_1 or γ_0 to the curve Γ is along the normal. Denote the value of the parameter of the curve at the foot of this normal as s, and the distance between the original point and the foot of the normal as n, see Fig. 5. As the position of the point may be on either side of the curve, the value of the distance n is taken with the sign: $n > 0$ corresponds

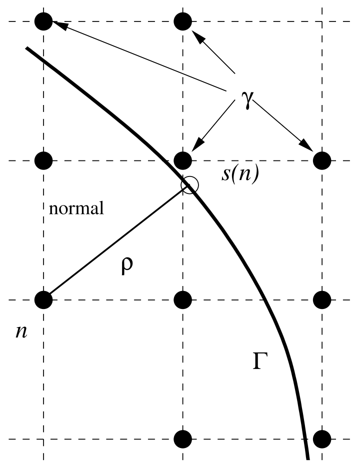

Fig. 5. New coordinates (n, s) and equation-based extension.

to the positive direction $\boldsymbol{\nu}$, i.e., to the exterior of Ω_1 (toward Ω_0), and $n < 0$ corresponds to the negative direction of $\boldsymbol{\nu}$, i.e., to the interior of Ω_1. The pair of numbers (n, s) provides the orthogonal coordinates that identify the location of a given point on the plane.

For a general shape of the boundary Γ the coordinates (n, s) may be prone to some ambiguity, as multiple shortest normals may exist for some of the nodes. Therefore, the multi-valued distance function at such nodes is non-differentiable with respect to the arc length s. The multiple shortest distances for a given node may occur when the minimum radius of curvature $\bar{R} = \min_s R(s)$ is of order h since the coordinates (n, s) are used only for the points of the grid boundary γ which are all about one grid size h away from the curve Γ, see Figs. 2, 4 and 5. This implies that the grid does not adequately resolve the geometry, and needs to be refined. The simulations in this paper, see Section 6, do not involve shapes with the features where the curvature $\zeta \sim h^{-1}$. In the future, we hope to analyze shapes with "small" features.

The formulae hereafter are all extensions of those obtained in [13,14] for circular and elliptical obstacles. The coordinates (n, s) are orthogonal but not necessarily orthonormal. For a given point (n, s), its radius-vector $\boldsymbol{r}$ is expressed as follows:

$$\begin{aligned}\boldsymbol{r} = \boldsymbol{r}(n, s) = \boldsymbol{R}(s) + n\boldsymbol{\nu}(s) =& (R_x(s) + n\nu_x(s), R_y(s) + n\nu_y(s))\\ =& \Big(R_x + n\frac{dR_y}{ds}, R_y - n\frac{dR_x}{ds}\Big).\end{aligned}$$

Consequently, the basis vectors are given by

$$\boldsymbol{e}_1 = \frac{\partial \boldsymbol{r}}{\partial n} = \Big(\frac{dR_y}{ds}, -\frac{dR_x}{ds}\Big) = (\tau_y, -\tau_x) = \boldsymbol{\nu}$$

and

$$\begin{aligned}\boldsymbol{e}_2 = \frac{\partial \boldsymbol{r}}{\partial s} =& \Big(\frac{dR_x}{ds} + n\frac{d^2R_y}{ds^2}, \frac{dR_y}{ds} - n\frac{d^2R_x}{ds^2}\Big)\\ =& \Big(\frac{dR_x}{ds} + n\zeta\nu_y, \frac{dR_y}{ds} - n\zeta\nu_x\Big)\\ =& (\tau_x - n\zeta\tau_x, \tau_y - n\zeta\tau_y) = (1 - n\zeta)\boldsymbol{\tau},\end{aligned}$$

where we have used formulae (22), (23), and (24). Accordingly, the Lame coefficients for the coordinates (n, s) are

$$H_1 \equiv H_n = |\boldsymbol{e}_1| = 1$$

and

$$H_2 \equiv H_s = |\boldsymbol{e}_2| = |1 - n\zeta| = 1 - n\zeta, \tag{25}$$

where the last equality in (25) holds because $n < \zeta^{-1}$ for $\zeta > 0$ and $n > \zeta^{-1}$ for $\zeta < 0$ (otherwise, the minimum radius of curvature $\bar{R}$ may be of order h or smaller).

In the coordinates (n, s), the Helmholtz equation becomes

$$\frac{1}{H_s}\left[\frac{\partial}{\partial n}\left(H_s\frac{\partial u}{\partial n}\right) + \frac{\partial}{\partial s}\left(\frac{1}{H_s}\frac{\partial u}{\partial s}\right)\right] + k^2(n, s)u = f, \tag{26}$$

where $H_s = H_s(n, s)$ is given by (25), and we have taken into account that $H_n \equiv 1$. Eq. (26) will be used for building the equation-based extension of a given $\boldsymbol{\xi}_\Gamma$ from the continuous boundary Γ to the nodes of the grid boundaries γ_1 and γ_0. If, in particular, Γ is a circle of radius R, then the foregoing general constructs transform into the corresponding constructs for polar coordinates [13,14]. In this case, the curvature ζ of (24) does not depend on s:

$$\zeta = -\frac{1}{R},$$

and consequently [see formula (25)],

$$H_s = 1 + \frac{n}{R} = \frac{R+n}{R} = \frac{r}{R}.$$

Then, according to (26), we can write:

$$\Delta u = \frac{R}{r}\left[\frac{\partial}{\partial n}\left(\frac{r}{R}\frac{\partial u}{\partial n}\right) + \frac{\partial}{\partial s}\left(\frac{R}{r}\frac{\partial u}{\partial s}\right)\right] = \frac{1}{r}\frac{\partial}{\partial n}\left(r\frac{\partial u}{\partial n}\right) + \frac{R^2}{r^2}\frac{\partial^2 u}{\partial s^2}.$$

Finally, we have $n = r - R$ so that $\frac{\partial}{\partial n} = \frac{\partial}{\partial r}$, and $s = R\theta$ so that $\frac{\partial}{\partial s} = \frac{1}{R}\frac{\partial}{\partial \theta}$, which yields:

$$\Delta u = \frac{1}{r}\frac{\partial}{\partial r}\left(r\frac{\partial u}{\partial r}\right) + \frac{1}{r^2}\frac{\partial^2 u}{\partial \theta^2}.$$

5.2. Equation-based extension

Given $\boldsymbol{\xi}_\Gamma$, we define a new smooth function $v = v(n, s)$ in the vicinity of Γ by means of the Taylor formula:

$$v(n, s) = v(0, s) + \sum_{l=1}^{L} \frac{1}{l!}\frac{\partial^l v(0, s)}{\partial n^l} n^l. \tag{27}$$

The zeroth and first order derivatives in (27) coincide with the respective components of $\boldsymbol{\xi}_\Gamma$:

$$v(0, s) = \xi_0(s) \quad \text{and} \quad \frac{\partial v(0, s)}{\partial n} = \xi_1(s).$$

All higher order derivatives in formula (27) are determined with the help of Eq. (26) applied to v. We multiply both sides of (26) by H_s and obtain

$$H_s\frac{\partial^2 v}{\partial n^2} + \frac{\partial H_s}{\partial n}\frac{\partial v}{\partial n} + \left(\frac{\partial}{\partial s}\frac{1}{H_s}\right)\frac{\partial v}{\partial s} + \frac{1}{H_s}\frac{\partial^2 v}{\partial s^2} + H_s k^2 v = H_s f,$$

where $\frac{\partial H_s}{\partial n} = -\zeta(s)$ and $\frac{\partial}{\partial s}\frac{1}{H_s} = \frac{n}{H_s^2}\zeta'(s)$, see formula (25). Then, we solve for the second derivative with respect to n, which yields:

$$\frac{\partial^2 v}{\partial n^2} = f(n, s) - k^2(n, s)v + \frac{\zeta}{H_s}\frac{\partial v}{\partial n} - \frac{n\zeta'(s)}{H_s^3}\frac{\partial v}{\partial s} - \frac{1}{H_s^2}\frac{\partial^2 v}{\partial s^2}. \tag{28}$$

Consequently,

$$\frac{\partial^2 v(0, s)}{\partial n^2} = f(0, s) - k^2(0, s)\xi_0(s) + \zeta(s)\xi_1(s) - \frac{\partial^2 \xi_0(s)}{\partial s^2}.$$

Next, we differentiate Eq. (28) with respect to n:

$$\begin{aligned}
\frac{\partial^3 v}{\partial n^3} &= \frac{\partial f}{\partial n} - k^2\frac{\partial v}{\partial n} - 2k\frac{\partial k}{\partial n}v + \left(\frac{\partial}{\partial n}\frac{1}{H_s}\right)\zeta\frac{\partial v}{\partial n} + \frac{\zeta}{H_s}\frac{\partial^2 v}{\partial n^2} \\
&\quad - \zeta'\left(\frac{1}{H_s^3} + n\left(\frac{\partial}{\partial n}\frac{1}{H_s^3}\right)\right)\frac{\partial v}{\partial s} - \left(\frac{\partial}{\partial n}\frac{1}{H_s^2}\right)\frac{\partial^2 v}{\partial s^2} - \frac{n\zeta'}{H_s^3}\frac{\partial^2 v}{\partial n \partial s} - \frac{1}{H_s^2}\frac{\partial^3 v}{\partial n \partial s^2} \\
&= \frac{\partial f}{\partial n} - k^2\frac{\partial v}{\partial n} - 2k\frac{\partial k}{\partial n}v + \frac{\zeta^2}{H_s^2}\frac{\partial v}{\partial n} + \frac{\zeta}{H_s}\frac{\partial^2 v}{\partial n^2} \\
&\quad - \zeta'\left(\frac{1}{H_s^3} + n\left(\frac{\partial}{\partial n}\frac{1}{H_s^3}\right)\right)\frac{\partial v}{\partial s} - \frac{2\zeta}{H_s^3}\frac{\partial^2 v}{\partial s^2} - \frac{n\zeta'}{H_s^3}\frac{\partial^2 v}{\partial n \partial s} - \frac{1}{H_s^2}\frac{\partial^3 v}{\partial n \partial s^2}
\end{aligned} \tag{29}$$

and substitute $n = 0$ to get:

$$\frac{\partial^3 v(0, s)}{\partial n^3} = \frac{\partial f}{\partial n} - 2k\frac{\partial k}{\partial n}\xi_0(s) + \left(\zeta^2 - k^2\right)\xi_1(s) + \zeta\frac{\partial^2 v(0, s)}{\partial n^2} - \zeta'\frac{\partial \xi_0(s)}{\partial s} - 2\zeta\frac{\partial^2 \xi_0(s)}{\partial s^2} - \frac{\partial^2 \xi_1(s)}{\partial s^2}.$$

Similarly, the fourth normal derivative is obtained by differentiating (29) with respect to n:

$$\frac{\partial^4 v}{\partial n^4} = \frac{\partial^2 f}{\partial n^2} - 2\left(\left(\frac{\partial k}{\partial n}\right)^2 + k\frac{\partial^2 k}{\partial n^2}\right) v + \left(\frac{2\zeta^3}{H_s^3} - 4k\frac{\partial k}{\partial n}\right)\frac{\partial v}{\partial n} + \left(2\frac{\zeta^2}{H_s^2} - k^2\right)\frac{\partial^2 v}{\partial n^2}$$
$$+ \frac{\zeta}{H_s}\frac{\partial^3 v}{\partial n^3} - \frac{3\zeta\zeta'}{H_s^4}\left(\frac{\partial v}{\partial s} + n\left(\frac{\partial^2 v}{\partial s \partial n} + \frac{3\zeta}{H_s}\frac{\partial v}{\partial s}\right)\right) - \frac{6\zeta^2}{H_s^4}\frac{\partial^2 v}{\partial s^2}$$
$$- \frac{\zeta'}{H_s^3}\left(2\frac{\partial^2 v}{\partial s\partial n} + \frac{3\zeta}{H_s}\frac{\partial v}{\partial s} + n\left(\frac{\partial^3 v}{\partial s \partial n^2} + \frac{3\zeta}{H_s}\frac{\partial^2 v}{\partial s\partial n} + \frac{3\zeta^2}{H_s^2}\frac{\partial v}{\partial s}\right)\right) - \frac{4\zeta}{H_s^3}\frac{\partial^3 v}{\partial n \partial s^2} - \frac{1}{H_s^2}\frac{\partial^4 v}{\partial n^2 \partial s^2}$$

and substituting $n = 0$, which yields:

$$\frac{\partial^4 v(0,s)}{\partial n^4} = \frac{\partial^2 f}{\partial n^2} - 2\left(\left(\frac{\partial k}{\partial n}\right)^2 + k\frac{\partial^2 k}{\partial n^2}\right)\xi_0(s) + \left(2\zeta^3 - 4k\frac{\partial k}{\partial n}\right)\xi_1(s) + \left(2\zeta^2 - k^2\right)\frac{\partial^2 v(0,s)}{\partial n^2}$$
$$+ \zeta\frac{\partial^3 v(0,s)}{\partial n^3} - 6\zeta\zeta'\frac{\partial \xi_0(s)}{\partial s} - 6\zeta^2\frac{\partial^2 \xi_0(s)}{\partial s^2} - 2\zeta'\frac{\partial \xi_1(s)}{\partial s} - 4\zeta\frac{\partial^2 \xi_1(s)}{\partial s^2} - \frac{\partial^4 v(0,s)}{\partial n^2 \partial s^2}.$$

The quantity $\frac{\partial^4 v(0,s)}{\partial n^2 \partial s^2}$ is derived by differentiating (28) twice with respect to s:

$$\frac{\partial^4 v}{\partial n^2 \partial s^2} = \frac{\partial^2 f}{\partial s^2} - 2\left(\left(\frac{\partial k}{\partial s}\right)^2 + k\frac{\partial^2 k}{\partial s^2}\right) v + \left(\frac{\zeta''}{H_s^2} + \frac{2n\left(\zeta'\right)^2}{H_s^3}\right)(H_s + n\zeta)\frac{\partial v}{\partial n}$$
$$- \left(\frac{n}{H_s^4}\left(H_s\zeta''' + 9n\zeta'\zeta'' + \frac{12n^2}{H_s}\left(\zeta'\right)^3\right) + 4k\frac{\partial k}{\partial s}\right)\frac{\partial v}{\partial s} - \left(\frac{4n\zeta''}{H_s^3} + \frac{12n^2\left(\zeta'\right)^2}{H_s^4} + k^2\right)\frac{\partial^2 v}{\partial s^2}$$
$$- \frac{5n\zeta'}{H_s^3}\frac{\partial^3 v}{\partial s^3} - \frac{1}{H_s^2}\frac{\partial^4 v}{\partial s^4} + 2\left(\frac{\zeta'}{H_s} + \frac{n\zeta\zeta'}{H_s^2}\right)\frac{\partial^2 v}{\partial n\partial s} + \frac{\zeta}{H_s}\frac{\partial^3 v}{\partial n \partial s^2}$$

and substituting $n = 0$:

$$\frac{\partial^4 v(0,s)}{\partial n^2 \partial s^2} = \frac{\partial^2 f}{\partial s^2} - 2\left(\left(\frac{\partial k}{\partial s}\right)^2 + k\frac{\partial^2 k}{\partial s^2}\right)\xi_0(s) + \zeta''\frac{\partial v}{\partial n}$$
$$- 4k\frac{\partial k}{\partial s}\frac{\partial \xi_0(s)}{\partial s} - k^2\frac{\partial^2 \xi_0(s)}{\partial s^2} - \frac{\partial^4 \xi_0(s)}{\partial s^4} + 2\zeta'\frac{\partial \xi_1(s)}{\partial s} + \zeta\frac{\partial^2 \xi_1(s)}{\partial s^2}.$$

Higher order derivatives (e.g., for the sixth order scheme) can be obtained in the same manner.

We emphasize that formula (27) is not an approximation of a given $v(n,s)$ by its truncated Taylor's expansion. It is rather the definition of a new function $v(n,s)$. This function is used for building the equation-based extension of $\boldsymbol{\xi}_\Gamma$ from Γ to γ_q:

$$\xi_{\gamma_q} = \boldsymbol{Ex}^{(q)}\boldsymbol{\xi}_\Gamma \stackrel{\text{def}}{=} v(n,s)\big|_{\gamma_q}. \tag{30}$$

In other words, extension (30) is obtained by drawing a normal from a given node of γ_p to Γ, see Fig. 5, and then using the Taylor formula with higher order derivatives computed by differentiating the governing equation (26).

6. Results

We consider the following problem [cf. formula (2)]:

$$\begin{cases} \Delta u + k_0^2 u = 0, & \boldsymbol{x} \in \Omega_0, \\ \Delta u + k_1(\boldsymbol{x})^2 u = 0, & \boldsymbol{x} \in \Omega_1, \\ \Delta u + k_2(\boldsymbol{x})^2 u = 0, & \boldsymbol{x} \in \Omega_2, \end{cases} \tag{31}$$

driven by the incident wave $u^{(\text{inc})} = e^{ik_0 R_x \cos\theta + ik_0 R_y \sin\theta}$, where θ denotes the angle of incidence. The wavenumber for the exterior domain Ω_0 is constant while the wavenumber for the interior Ω_2 and intermediate Ω_1 domains varies:

$$k_q(\boldsymbol{x}) = \tilde{k}_q e^{-10(r-r_0)^6 r^6}, \quad q \in \{1,2\}, \tag{32}$$

where $r_0 = 1.6$ and $\tilde{k}_1$ is a parameter that assumes different values for different simulations described below. In what follows, except for the last example, we solve a simplified problem (31) for several irregular shapes of the interface $\Gamma = \Gamma_1 = \{\boldsymbol{R}(s) = (R_x(s), R_y(s))\}$ between Ω_0 and Ω_1, with no additional interface Γ_2 inside Γ_1. In the last example,

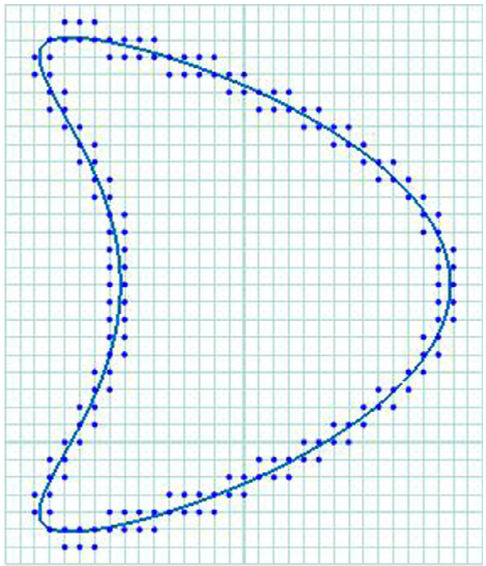

(a) Cartesian grid.

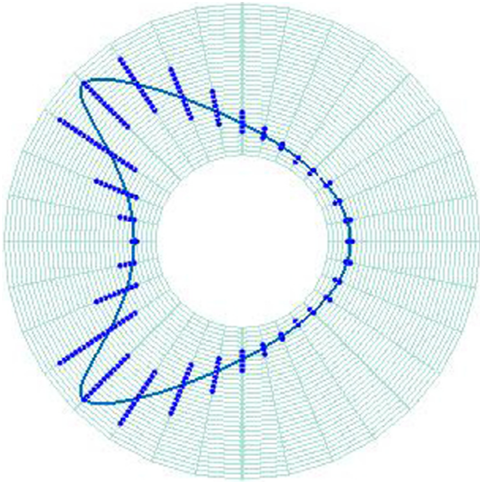

(b) Polar grid.

Fig. 6. The grid boundaries for the kite on a 33×33 discretization grid.

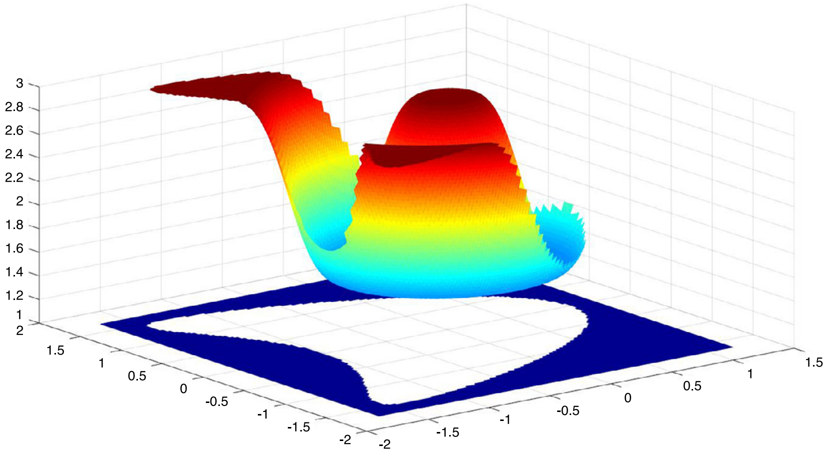

(a) $k_0 = 1$ and $\tilde{k}_1 = 3$.

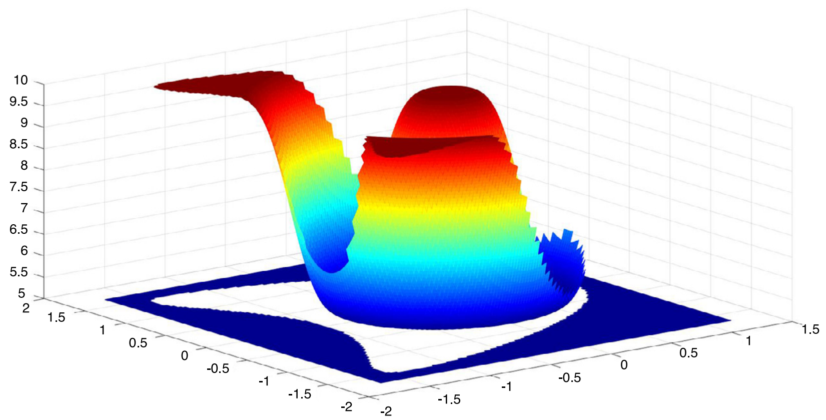

(b) $k_0 = 5$ and $\tilde{k}_1 = 10$.

Fig. 7. The wave number k for the kite.

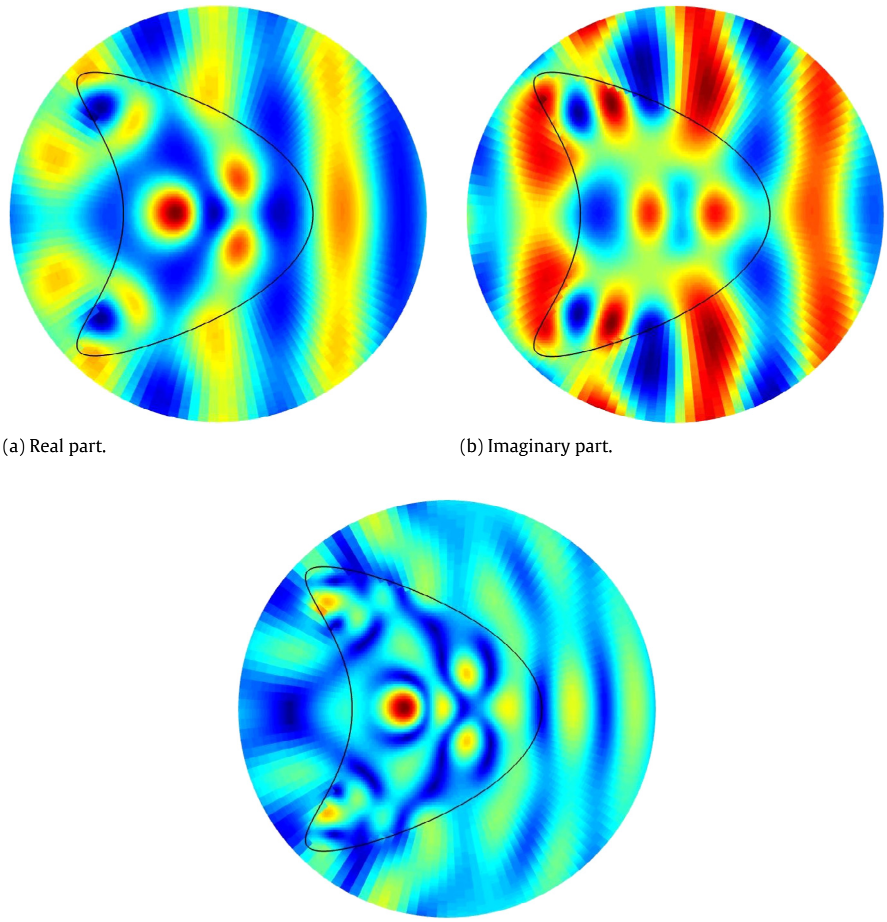

(a) Real part.

(b) Imaginary part.

(c) Absolute value.

Fig. 8. Total field for the transmission and scattering of a plane wave about a kite at the angle of incidence $\theta = 0°$, with $k_0 = 5$ and $\tilde{k}_1 = 10$.

Table 1
Fourth order grid convergence for the transmission and scattering of a plane wave with the incidence angle $\theta = 0°$ about a kite.

Grid	$k_0 = 1, \tilde{k}_1 = 3, M = 61$		$k_0 = 5, \tilde{k}_1 = 10, M = 64$		$k_0 = 10, \tilde{k}_1 = 20, M = 67$	
	$\Vert u^h - u^{2h} \Vert_\infty$	Rate	$\Vert u^h - u^{2h} \Vert_\infty$	Rate	$\Vert u^h - u^{2h} \Vert_\infty$	Rate
	Exterior					
64 × 64	6.294093e+00	–	5.261709e+03	–	1.869403e+03	–
128 × 128	5.798326e−03	10.08	7.493228e−01	12.78	2.575746e+00	9.50
256 × 256	5.719824e−04	3.34	8.757690e−03	6.42	1.919236e−01	3.75
512 × 512	1.484623e−05	5.27	5.326607e−04	4.04	3.126876e−03	5.94
1024 × 1024	8.515695e−07	4.12	2.078834e−05	4.68	2.377990e−04	3.72
2049 × 2049	3.917679e−08	4.44	1.011240e−06	4.36	1.242605e−05	4.26
	Interior					
64 × 64	4.148434e+01	–	1.406104e+05	–	1.224631e+04	–
128 × 128	3.156142e−02	10.36	3.398898e+00	15.34	3.117782e+00	11.94
256 × 256	4.703980e−03	2.75	1.131129e−01	4.91	8.350206e−01	1.90
512 × 512	2.095950e−05	7.81	6.704542e−04	7.40	5.691779e−03	7.20
1024 × 1024	7.021794e−07	4.90	1.839269e−05	5.19	2.207484e−04	4.69
2049 × 2049	4.131632e−08	4.09	9.240163e−07	4.32	8.825747e−06	4.64

we solve a full fledged formulation with two interfaces, Γ_2 and Γ_1, and multiple scattering. Since the exact solution u of problem (31) is typically not known, we cannot directly observe or quantify the grid convergence:

$$\Vert u - u^{(h)} \Vert \to 0 \quad \text{as } h \to 0, \tag{33}$$

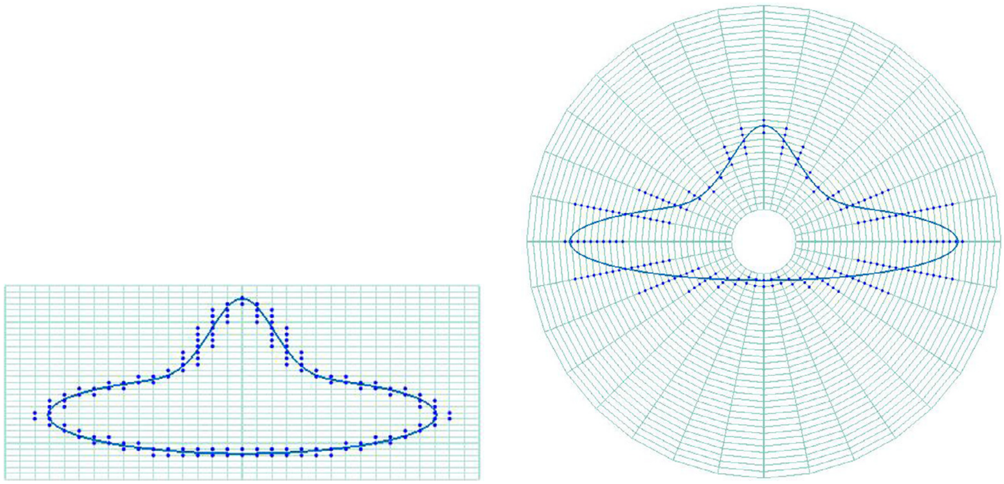

(a) Cartesian grid. (b) Polar grid.

Fig. 9. The grid boundaries for the submarine on a 33 × 33 discretization grid.

Table 2
Fourth order grid convergence for the transmission and scattering of a plane wave about a submarine at the angle of incidence $\theta = 0°$.

Grid	$k_0 = 1, \tilde{k}_1 = 3, M = 90$		$k_0 = 5, \tilde{k}_1 = 10, M = 95$		$k_0 = 10, \tilde{k}_1 = 20, M = 100$	
	$\Vert u^h - u^{2h}\Vert_\infty$	Rate	$\Vert u^h - u^{2h}\Vert_\infty$	Rate	$\Vert u^h - u^{2h}\Vert_\infty$	Rate
	Exterior					
64 × 64	2.295752e+01	–	2.237487e+00	–	9.916726e−01	–
128 × 128	1.375159e+02	−2.58	1.619068e+03	−9.50	3.583345e+05	−18.46
256 × 256	4.990559e−01	8.11	3.935502e+00	8.68	2.036714e+00	17.42
512 × 512	1.290265e−03	8.60	8.432259e−03	8.87	3.475999e−02	5.87
1024 × 1024	1.293954e−05	6.64	6.619289e−05	6.99	1.481051e−04	7.87
2049 × 2049	4.003078e−07	5.01	2.210780e−06	4.90	5.048151e−06	4.87
	Interior					
64 × 64	7.864884e+00	–	9.351113e−01	–	9.979765e−01	–
128 × 128	4.266917e+03	−9.08	2.537239e+05	−18.05	3.109921e+07	−24.89
256 × 256	5.132072e−01	13.02	5.635594e+00	15.46	2.392006e+00	23.63
512 × 512	1.713991e−03	8.23	2.500136e−02	7.82	7.836997e−02	4.93
1024 × 1024	6.527788e−05	4.71	7.829261e−04	5.00	2.928307e−03	4.74
2049 × 2049	5.213601e−07	6.97	2.894848e−06	8.08	7.650070e−06	8.58

Table 3
Fourth order grid convergence for the external scattering of a plane wave about a submarine at the angle of incidence $\theta = 0°$.

Grid	$k_0 = 1, M = 95$		$k_0 = 5, M = 100$		$k_0 = 10, M = 105$	
	$\Vert u^h - u^{2h}\Vert_\infty$	Rate	$\Vert u^h - u^{2h}\Vert_\infty$	Rate	$\Vert u^h - u^{2h}\Vert_\infty$	Rate
64 × 64	1.051374e+08	–	1.052972e+07	–	8.293744e+05	–
128 × 128	1.259820e+01	22.99	6.467096e+01	17.31	1.716566e+02	12.24
256 × 256	6.211242e−03	10.99	1.791608e−02	11.82	4.192448e−02	12.00
512 × 512	6.969940e−04	3.16	1.789315e−03	3.32	3.971143e−03	3.40
1024 × 1024	4.196957e−05	4.05	9.784597e−05	4.19	2.377339e−04	4.06
2049 × 2049	1.841662e−06	4.51	5.761461e−06	4.09	1.159269e−05	4.36

where $u^{(h)}$ denotes the approximate solution obtained on the grid of size h. Instead, we assess the grid convergence by evaluating the norm of the difference between two succeeding approximate solutions obtained on a sequence of refined grids:

$$\Vert u^{(h)} - u^{(h/2)}\Vert \to 0 \quad \text{as } h \to 0. \tag{34}$$

Clearly, proper grid convergence in the sense of (33) implies (34). So, relation (34) provides a necessary condition for convergence. Moreover, if the actual convergence (33) is characterized by a certain rate, then the rate of convergence in the sense of (34) is at least as fast. Thus, all the examples that we present, in this section, show a fourth order convergence rate.

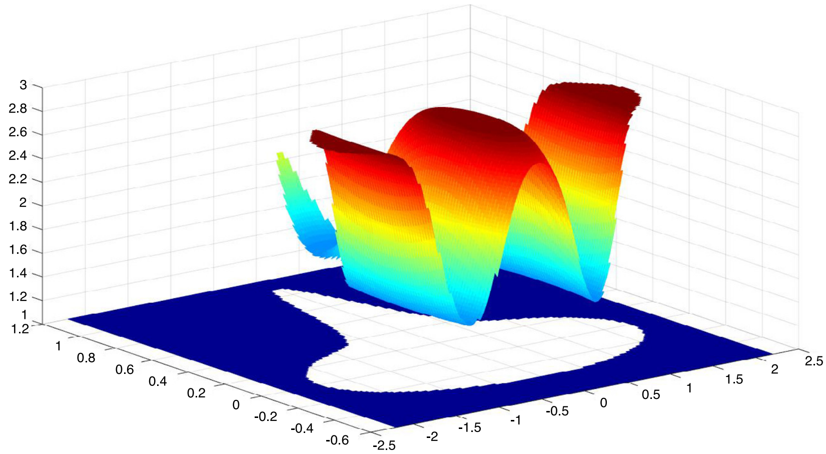

(a) $k_0 = 1$ and $\tilde{k}_1 = 3$.

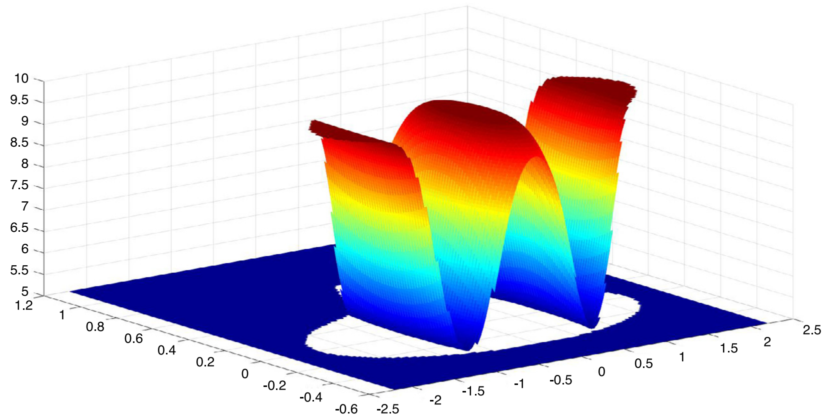

(b) $k_0 = 5$ and $\tilde{k}_1 = 10$.

Fig. 10. The wave number k for the submarine.

Table 4
Fourth order grid convergence for the transmission and scattering of a plane wave with the incidence angle $\theta = 0°$ about a star with rounded edges.

Grid	$k_0 = 1, \tilde{k}_1 = 3, M = 89$		$k_0 = 5, \tilde{k}_1 = 10, M = 97$		$k_0 = 10, \tilde{k}_1 = 20, M = 100$	
	$\Vert u^h - u^{2h}\Vert_\infty$	Rate	$\Vert u^h - u^{2h}\Vert_\infty$	Rate	$\Vert u^h - u^{2h}\Vert_\infty$	Rate
	Exterior					
64 × 64	1.897713e+01	–	1.359849e+01	–	4.464070e+02	–
128 × 128	6.274128e+00	1.60	6.472424e+00	1.07	4.617413e+02	−0.05
256 × 256	2.693255e−03	11.19	7.835759e−03	9.69	7.305258e−02	12.63
512 × 512	1.266509e−05	7.73	1.072922e−04	6.19	5.144006e−04	7.15
1024 × 1024	6.169030e−07	4.36	4.556798e−06	4.56	2.833560e−05	4.18
2049 × 2049	3.215375e−08	4.26	3.142369e−07	3.86	1.436230e−06	4.30
	Interior					
64 × 64	3.440719e+02	–	3.558703e+02	–	9.670006e+03	–
128 × 128	1.784930e+01	4.27	2.146546e+01	4.05	1.611719e+03	2.58
256 × 256	3.058072e−03	12.51	2.875988e−02	9.54	1.764544e−01	13.16
512 × 512	1.251820e−05	7.93	3.272978e−04	6.46	1.063229e−03	7.37
1024 × 1024	6.189435e−07	4.34	4.147246e−06	6.30	2.641565e−05	5.33
2049 × 2049	3.395252e−08	4.19	3.026219e−07	3.78	1.437789e−06	4.20

Relation (34) does not provide a sufficient condition for the true convergence in the sense of (33). Rather (34) is similar to convergence in the sense of Cauchy.[2] However, condition (34) is easy to check, in a practical setting, when no exact solution is available. Therefore, we shall use it as a convergence indicator. The norm in (34) is chosen as the maximum norm, $\Vert \cdot \Vert_\infty$.

[2] Condition (34) is somewhat weaker than convergence in the sense of Cauchy, because we only consider pairs of succeeding grids $(h, h/2)$ rather than all the grids finer than a given h.

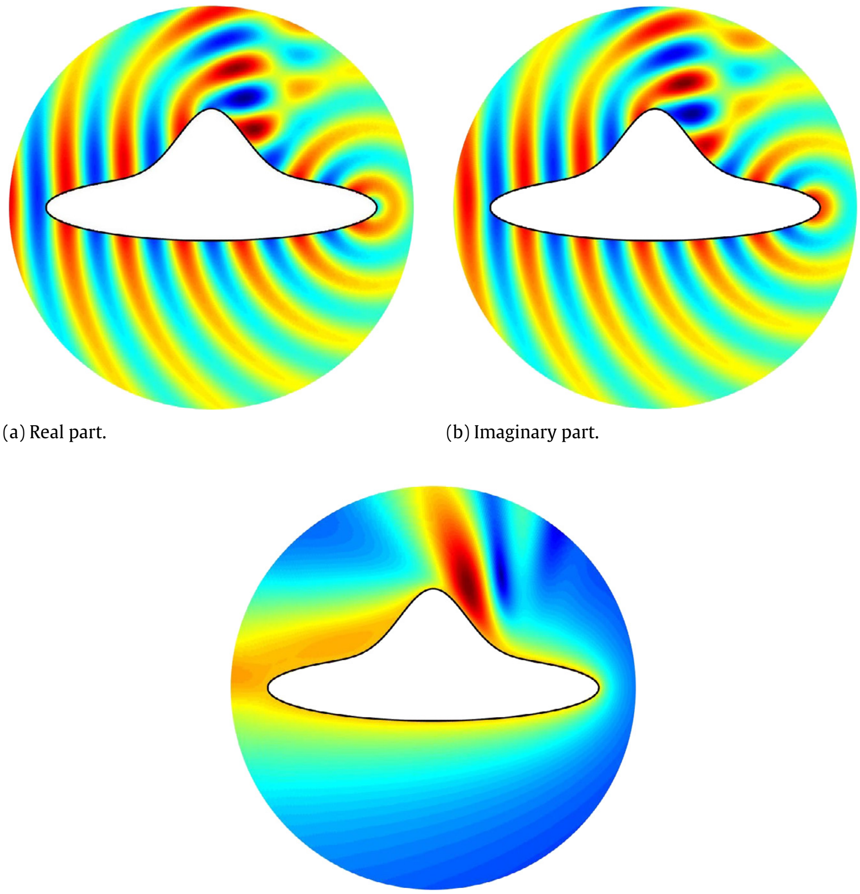

(a) Real part.

(b) Imaginary part.

(c) Absolute value.

Fig. 11. Scattered field for the external scattering of a plane wave about a submarine at the angle of incidence $\theta = 0^\circ$ and with $k_0 = 10$.

6.1. A kite

The first case is an interface in the form of a kite given by:

$$\Gamma = \boldsymbol{R}(t) = \left(R_x(t), R_y(t)\right) = \left(\cos t + 0.65\cos 2t - 0.65,\ 1.5\sin t\right), \quad 0 \leqslant t \leqslant 2\pi.$$

For the interior auxiliary problem, we take a Cartesian grid on the rectangle $[-1.7, 1.2] \times [-1, 7, 1.7]$. For the exterior AP, we take a polar grid on the annulus $\{0.8 \leqslant r \leqslant 2.2\}$. The continuous boundary Γ and the grid boundaries γ_2 and γ_0 are shown in Fig. 6. Note, the auxiliary domain should allow for at least a few grid nodes between Γ and the outer boundary, so that the grid boundary γ_2 or γ_0 is fully inside the grid. The variable wave number for the entire domain is shown in Fig. 7 for two different cases: $k_0 = 1$ and $k_1 = k_1(\boldsymbol{x})$ given by (32) with $\tilde{k}_1 = 3$ in Fig. 7(a), and $k_0 = 5$, $\tilde{k}_1 = 10$ in Fig. 7(b). In Fig. 8 we display the solution driven by the plane wave at an angle of incidence $\theta = 0^\circ$. Table 1 presents the results for the grid convergence for three different choices of the exterior and interior wave number.

6.2. A submarine-like scatterer

Next we consider a submarine-like interface defined by:

$$\Gamma = \boldsymbol{R}(t) = (R_x(t), R_y(t)) = \left(1.8\cos t, 0.36\sin t \cdot \left(1 + 2\cdot\left(\frac{\cos\frac{t}{2} + \sin\frac{t}{2}}{\sqrt{2}}\right)^{150}\right)\right),$$

where $0 \leqslant t \leqslant 2\pi$. The interior AP is solved on the rectangle $[-2.2, 2.2] \times [-0, 6, 1.2]$ using a Cartesian grid. The exterior AP is solved on a polar grid in the annulus $\{0.3 \leqslant r \leqslant 2.2\}$. Fig. 9 presents the geometry of the interface Γ and the grid sets. Fig. 10 shows the variation of the wave number k across the computational domain for two cases: $k_0 = 1$ and $k_1 = k_1(\boldsymbol{x})$ with $\tilde{k}_1 = 3$ (see formula (32)) is in Fig. 10(a), and $k_0 = 5$, $k_1 = k_1(\boldsymbol{x})$ with $\tilde{k}_1 = 10$ is in Fig. 10(b).

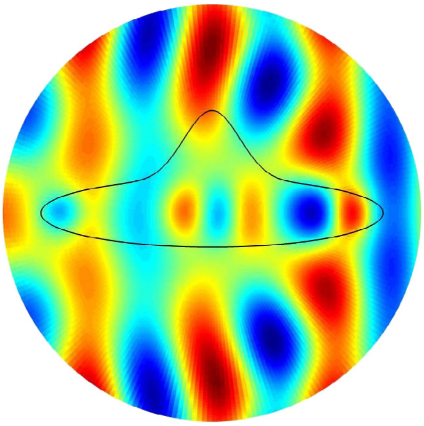

(a) Real part.

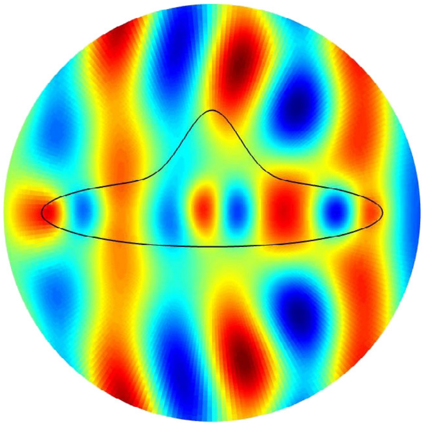

(b) Imaginary part.

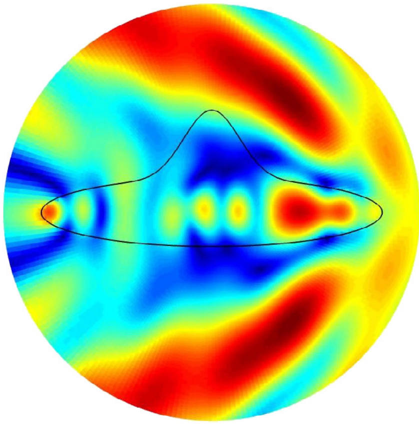

(c) Absolute value.

Fig. 12. Total field for the transmission and scattering of a plane wave about a submarine at the angle of incidence $\theta = 0^\circ$, with $k_0 = 5$ and $\tilde{k}_1 = 10$.

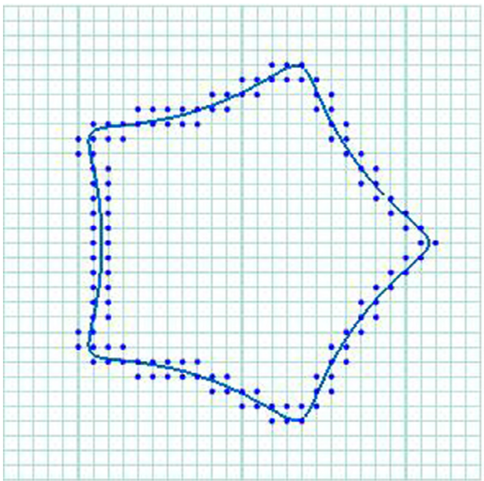

(a) Cartesian grid.

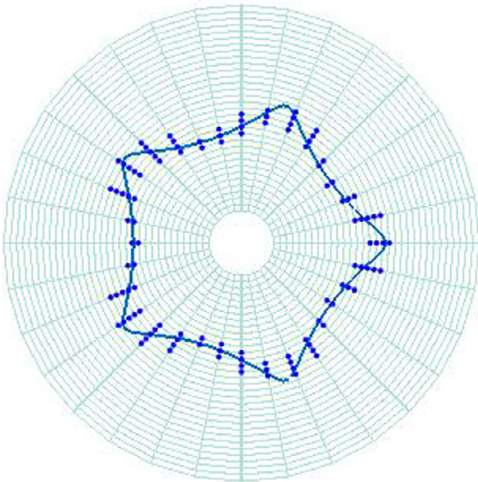

(b) Polar grid.

Fig. 13. The grid boundaries for the star with rounded edges on a 33×33 grid.

For the case of a submarine-like body, we solve two problems: an external scattering problem with a homogeneous Dirichlet boundary condition at the surface Γ and a transmission/scattering problem similar to that solved in Section 6.3

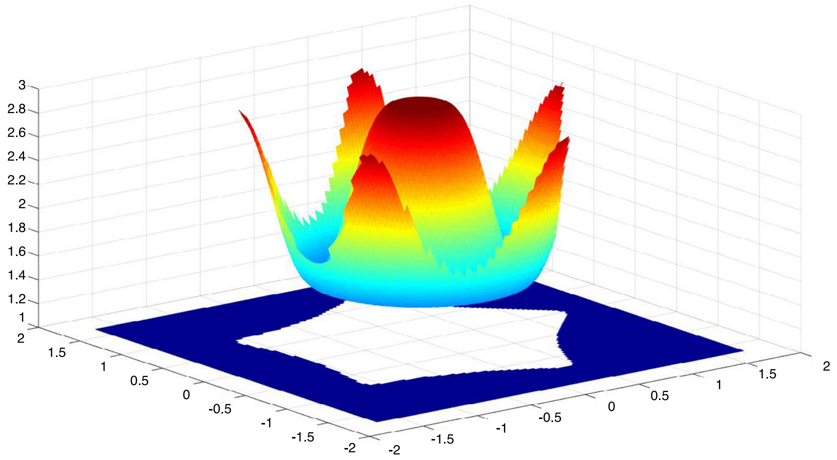

(a) $k_0 = 1$ and $\tilde{k}_1 = 3$.

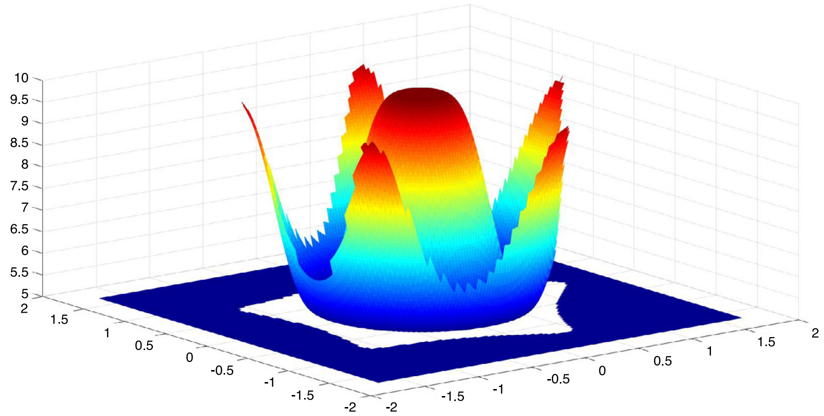

(b) $k_0 = 5$ and $\tilde{k}_1 = 10$.

Fig. 14. Profile of the variable wave number k for the star with rounded edges.

for the star interface and in Section 6.1 for the kite interface. The external scattering solution for $k_0 = 10$ and $\theta = 0°$ is presented in Fig. 11. Table 3 demonstrates the grid convergence for three different choices of the exterior wave number. The transmission/scattering solution for the submarine is shown in Fig. 12, while Table 2 summarizes the grid convergence results for this case.

6.3. A star with rounded edges

The third case is an interface shaped as a five-ray star with rounded edges to make it smooth. It is shown in Fig. 13 and is given by the following parametric expression:

$$\Gamma = \boldsymbol{R}(t) = (R_x(t), R_y(t)) = \left(\frac{1}{6}\cos(4t) + \frac{7}{6}\sin(t), \frac{7}{6}\cos(t) + \frac{1}{6}\sin(4t)\right), \quad 0 \leqslant t \leqslant 2\pi.$$

For the interior auxiliary problem, we choose a Cartesian grid on the square $[-1.7, 1.7] \times [-1, 7, 1.7]$. For the exterior AP, we choose a polar grid on the annulus $\{0.3 \leqslant r \leqslant 2.2\}$. The grid boundaries γ_2 and γ_0 defined by formulae (8) and (10), respectively, are also shown in Fig. 13 for the case where the dimension of the main discretization grid is 33×33. The variable wave number for the entire domain is shown in Fig. 14: specifically, in Fig. 14(a) the wave numbers are $k_0 = 1$ and $k_1 = k_1(\boldsymbol{x})$ with $\tilde{k}_1 = 3$, see formula (32), and in Fig. 14(b) we have $k_0 = 5$ and $\tilde{k}_1 = 10$. In Fig. 15, we present the solution for the incident plane wave at $\theta = 0°$. Table 4 demonstrates the grid convergence for various sets of parameters.

6.4. Multiple scattering

The last case is a multiple scattering problem, with interface $\Gamma = \Gamma_2 \cup \Gamma_1$ where Γ_2 is a five-ray star with rounded edges defined in the beginning of Section 6.3 and Γ_1 is a circle of radius $r = 2$. The schematic is shown in Fig. 16. For the

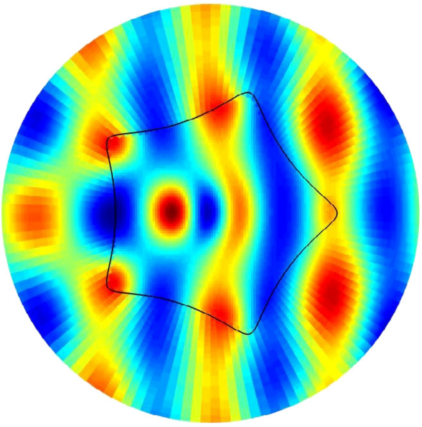

(a) Real part.

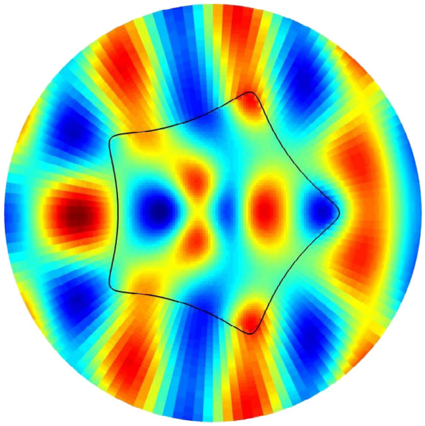

(b) Imaginary part.

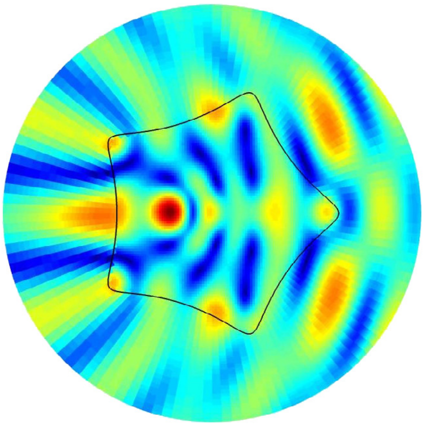

(c) Absolute value.

Fig. 15. Total field for the transmission and scattering of a plane wave about a star with rounded edges at the angle of incidence $\theta = 0^\circ$, with $k_0 = 5$ and $\tilde{k}_1 = 10$.

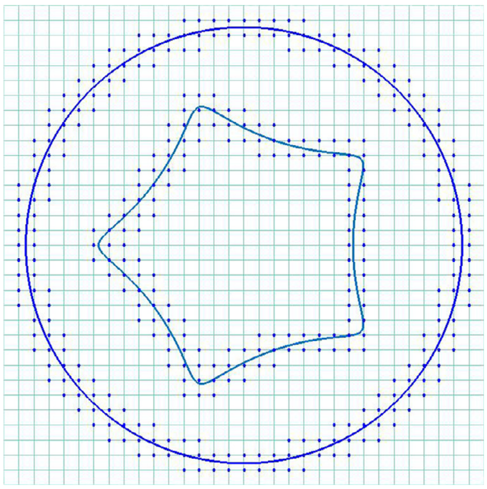

Fig. 16. The grid boundaries for the star with rounded edges inside a circle on a 33×33 grid.

exterior auxiliary problem, we choose a polar grid on the annulus $\{1.8 \leqslant r \leqslant 2.5\}$. For the interior auxiliary problem we choose exactly the same interior auxiliary problem as in Section 6.3, it is depicted in Fig. 13(a) and we choose a Cartesian grid on the square $[-1.7, 1.7] \times [-1.7, 1.7]$. For the intermediate auxiliary problem we choose a Cartesian grid on the

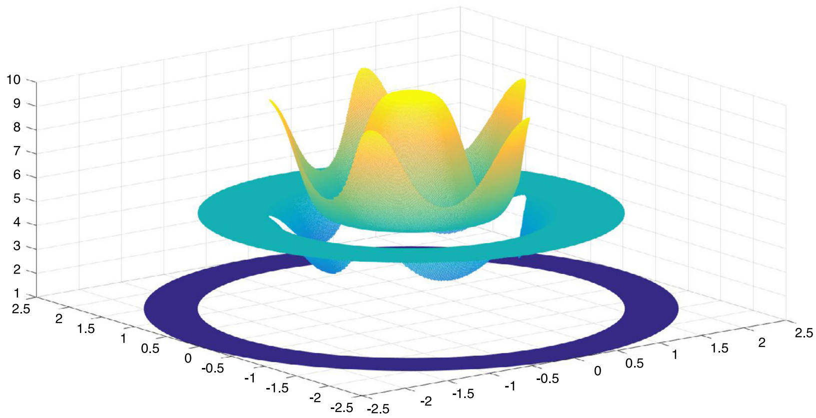

(a) $k_0 = 1$, $\tilde{k}_1 = 5$ and $\tilde{k}_2 = 10$.

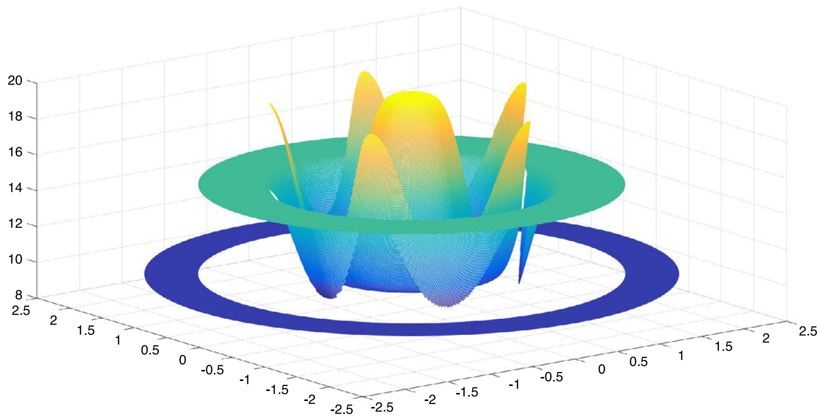

(b) $k_0 = 10$, $\tilde{k}_1 = 15$ and $\tilde{k}_2 = 20$.

Fig. 17. Profile of the variable wave number k for the star with rounded edges.

square $[-2.2, 2.2] \times [-2.2, 2.2]$. The grid boundaries γ_1 and γ_2 defined by formulae (8) and shown in Figs. 16 and 13(a) respectively, for the case where the dimension of the main discretization grid is 33×33. The grid boundary γ_0 is defined by (10). The variable wave number for the entire domain is shown in Fig. 17; see also Fig. 1 for the definition of k_0, k_1, and k_2. Specifically, in Fig. 17(a) the wave numbers are $k_0 = 1$, $k_1 = k_1(\boldsymbol{x})$, and $k_2 = k_2(\boldsymbol{x})$ with $\tilde{k}_1 = 5$ and $\tilde{k}_2 = 10$ respectively, see formula (32), and in Fig. 17(b) we have $k_0 = 20$, $\tilde{k}_1 = 50$, and $\tilde{k}_2 = 10$. In Fig. 18, we present the solution for the incident plane wave at $\theta = 40°$. Table 5 demonstrates the grid convergence for various sets of parameters.

7. Discussion

We have described a combined implementation of the method of difference potentials together with a compact high order accurate finite difference scheme for the numerical solution of wave propagation problems in the frequency domain for the case of general geometries. The Helmholtz equation is approximated on a regular structured grid, which is efficient and entails a low computational complexity. At the same time, the method of difference potentials guarantees no loss of accuracy for curvilinear non-conforming boundaries. We can also handle variable coefficients that describe a non-homogeneous medium. Thus, this methodology provides a viable alternative to both boundary element methods and high order finite element methods. Among the advantages of the proposed methodology are its capability to accurately reconstruct the solution and/or its normal derivative directly at the interface (without having to interpolate and/or use one-sided differences, such as done in conventional finite differences and finite elements).

The performance of our method and its design high order accuracy have been corroborated numerically by solving a variety of 2D transmission/scattering problems, including problems that involve multiple scattering, for smooth general shaped domains with a varying wavenumber using only Cartesian and polar grids.

The case of general shaped domains with the boundaries that are not necessarily smooth has not been investigated in the paper. There are two main differences between this case and the case of smooth boundaries that we have analyzed. On one

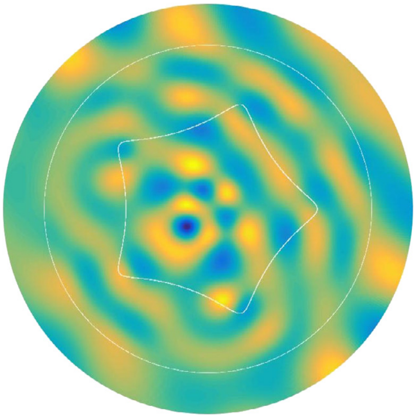

(a) Real part.

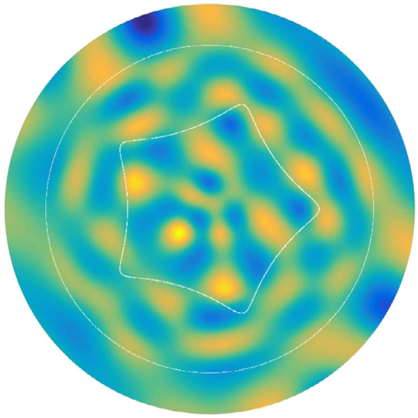

(b) Imaginary part.

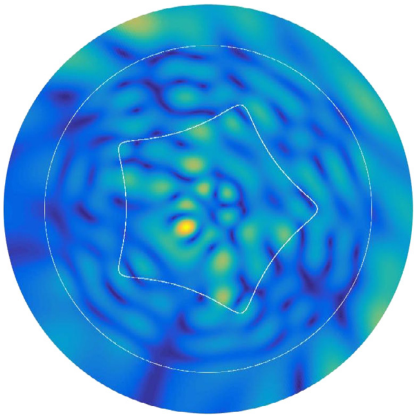

(c) Absolute value.

Fig. 18. Total field for the transmission and scattering of a plane wave about a star with rounded edges inside circle at angle of incidence $\theta = 40°$, with $k_0 = 5, \tilde{k}_1 = 10$ and $\tilde{k}_2 = 15$.

Table 5
Fourth order grid convergence for the multiple scattering of a plane wave with the incidence angle $\theta = 40°$ through a star with rounded edges inside circle.

Grid	$k_0 = 1, \tilde{k}_1 = 5, \tilde{k}_2 = 10, M = 90$		$k_0 = 5, \tilde{k}_1 = 10, \tilde{k}_2 = 15, M = 96$		$k_0 = 10, \tilde{k}_1 = 15, \tilde{k}_2 = 20, M = 101$	
	$\|u^h - u^{2h}\|_\infty$	Rate	$\|u^h - u^{2h}\|_\infty$	Rate	$\|u^h - u^{2h}\|_\infty$	Rate
	Exterior					
64 × 64	8.576803e+00	–	8.452339e+00	–	4.131025e+00	–
128 × 128	9.166389e+00	−0.10	4.221633e+00	1.00	1.989940e+00	1.05
256 × 256	2.558925e−03	11.81	1.578030e−03	11.39	2.085242e−02	6.58
512 × 512	9.164032e−05	4.80	6.357957e−05	4.63	8.377927e−04	4.64
1024 × 1024	6.080010e−06	3.91	3.995037e−06	3.99	5.260751e−05	3.99
2049 × 2049	3.442998e−07	4.14	2.587757e−07	3.95	3.278522e−06	4.00
	Intermediate					
64 × 64	3.625781e+01	–	7.146890e+03	–	3.489656e+03	–
128 × 128	5.437903e+01	−0.58	1.871236e+03	1.93	1.341972e+03	1.38
256 × 256	3.890433e−03	13.77	8.918431e−03	17.68	9.264290e−02	13.82
512 × 512	1.327692e−04	4.87	6.825677e−05	7.03	9.212461e−04	6.65
1024 × 1024	8.830146e−06	3.91	4.288235e−06	3.99	5.759067e−05	4.00
2049 × 2049	4.962013e−07	4.15	2.776753e−07	3.95	3.595732e−06	4.00
	Interior					
64 × 64	6.798173e+02	–	8.037889e+04	–	1.666677e+05	–
128 × 128	6.253578e+02	0.12	1.434150e+04	2.49	8.019034e+04	1.06
256 × 256	4.137007e−03	17.21	5.293907e−03	21.37	7.849041e−02	19.96
512 × 512	1.411678e−04	4.87	8.649081e−05	5.94	3.729582e−04	7.72
1024 × 1024	9.542619e−06	3.89	2.919410e−06	4.89	2.282353e−05	4.03
2049 × 2049	5.394062e−07	4.14	1.913741e−07	3.93	1.489259e−06	3.94

hand, if the boundary is only piece-wise smooth rather than smooth (e.g., it has corners), then the systems of basis functions (Section 4.2), as well as the curvilinear coordinates and equation-based extensions (Section 5), need to be constructed independently for each smooth interval of the boundary. Other components of the method of difference potentials, such as the auxiliary problem and the definitions of the grid sets (Section 4.1), remain unaffected. Altogether, the corresponding modifications are substantial but well understood. They have been introduced and successfully tested previously in the work [15], where we studied problems with non-standard boundary conditions (e.g., Dirichlet on one part of the boundary and Neumann on the other part of the boundary), and in the work [16], where we allowed for discontinuous boundary data. On the other hand, in the case of a boundary with corners (in particular, re-entrant corners), the solution itself frequently becomes singular. For singular solutions, the finite difference schemes of Section 3 (as well as many other schemes) will no longer be consistent, and the overall solution accuracy will deteriorate or may even be completely lost. To avoid this, the solution needs to be regularized prior to having it approximated numerically. This is what we did in the work [16], where the singularities in the solution were due to discontinuities in the boundary data. The regularization was done by truncating several leading terms of the asymptotic expansion near the singularity. We then obtained the design fourth order accuracy of the numerical method. When the singularities are due to the geometric features of the boundary, the regularization of the solution proves more subtle because a certain part of the regularizing expansion cannot be determined ahead of time. This issue requires a thorough investigation that is beyond the scope of the current work. Once complete, the results will be presented in a separate publication.

References

[1] A. Bayliss, C.I. Goldstein, E. Turkel, On accuracy conditions for the numerical computation of waves, J. Comput. Phys. 59 (3) (1985) 396–404.
[2] F. Ihlenburg, Finite Element Analysis of Acoustic Scattering, in: Applied Mathematical Sciences, vol. 132, Springer, 1998.
[3] I.M. Babuska, S.A. Sauter, Is the pollution effect of the FEM avoidable for the Helmholtz equation considering high wave numbers? SIAM J. Numer. Anal. 34 (6) (1997) 2392–2423.
[4] S. Britt, S. Tsynkov, E. Turkel, A compact fourth order scheme for the Helmholtz equation in polar coordinates, J. Sci. Comput. 45 (1–3) (2010) 26–47.
[5] S. Britt, S. Tsynkov, E. Turkel, Numerical simulation of time-harmonic waves in inhomogeneous media using compact high order schemes, Commun. Comput. Phys. 9 (3) (2011) 520–541.
[6] V.S. Ryaben'kii, Boundary equations with projections, Russian Math. Surveys 40 (2) (1985) 147–183.
[7] V.S. Ryaben'kii, Method of Difference Potentials and Its Applications, in: Springer Series in Computational Mathematics, vol. 30, Springer-Verlag, Berlin, 2002.
[8] I. Harari, E. Turkel, Accurate finite difference methods for time-harmonic wave propagation, J. Comput. Phys. 119 (2) (1995) 252–270.
[9] I. Singer, E. Turkel, High-order finite difference methods for the Helmholtz equation, Comput. Methods Appl. Mech. Engrg. 163 (1–4) (1998) 343–358.
[10] I. Singer, E. Turkel, Sixth-order accurate finite difference schemes for the Helmholtz equation, J. Comput. Acoust. 14 (3) (2006) 339–351.
[11] G. Sutmann, Compact finite difference schemes of sixth order for the Helmholtz equation, J. Comput. Appl. Math. 203 (1) (2007) 15–31.
[12] M. Nabavi, K. Siddiqui, J. Dargahi, A new 9-point sixth-order accurate compact finite-difference method for the Helmholtz equation, J. Sound Vib. 307 (2007) 972–982.
[13] M. Medvinsky, S.V. Tsynkov, E. Turkel, The method of difference potentials for the Helmholtz equation using compact high order schemes, J. Sci. Comput. 53 (1) (2012) 150–193.
[14] M. Medvinsky, S.V. Tsynkov, E. Turkel, High order numerical simulation of the transmission and scattering of waves using the method of difference potentials, J. Comput. Phys. 243 (2013) 305–322.
[15] S. Britt, S. Tsynkov, E. Turkel, A High-Order numerical method for the Helmholtz equation with non-standard boundary conditions, SIAM J. Sci. Comput. 35 (5) (2013) A2255–A2292.
[16] S. Britt, S. Petropavlovsky, S. Tsynkov, E. Turkel, Computation of singular solutions to the Helmholtz equation with high order accuracy, Appl. Numer. Math. 93 (2015) 215–241.
[17] M. Medvinsky, Y. Epshteyn, On the solution of the elliptic interface problems by difference potentials method, in: Springer volume of LNCSE Series, vol. 106, 2015, pp. 197–205.
[18] J. Albright, Y. Epshteyn, M. Medvinsky, Q. Xia, High-order numerical schemes based on difference potentials for 2D elliptic problems with material interfaces (submitted for publication), 2015.
[19] A.P. Calderon, Boundary-value problems for elliptic equations, in: Proceedings of the Soviet-American Conference on Partial Differential Equations at Novosibirsk, Fizmatgiz, Moscow, 1963, pp. 303–304.
[20] R.T. Seeley, Singular integrals and boundary value problems, Amer. J. Math. 88 (1966) 781–809.
[21] E. Turkel, D. Gordon, R. Gordon, S.V. Tsynkov, Compact 2D and 3D Sixth Order Schemes for the Helmholtz Equation with Variable Wave Number, J. Comput. Phys. 232 (1) (2013) 272–287.
[22] M. Medvinsky, High order numerical simulation of waves using regular grids and non-conforming interfaces (Ph.D. Dissertation), Tel Aviv University, 2013.
[23] A.A. Reznik, Approximation of surface potentials of elliptic operators by difference potentials, Dokl. Akad. Nauk SSSR 263 (6) (1982) 1318–1321.
[24] A.C. Cangellaris, D.B. Wright, Analysis of the numerical error caused by the stair-stepped approximation of a conducting boundary in FDTD simulations of electromagnetic phenomena, IEEE Trans. Antennas and Propagation 39 (10) (1991) 1518–1525.
[25] R. Holland, Pitfalls of staircase meshing, IEEE Trans. Electromagn. Compat. 35 (1993) 434–439.
[26] S.P. Novikov, A.T. Fomenko, Basic Elements of Differential Geometry and Topology, in: Mathematics and its Applications (Soviet Series), vol. 60, Kluwer Academic Publishers Group, Dordrecht, 1990, Translated from the Russian by M. V. Tsaplina.